Contemporary Mathematics
http://ojs.wiserpub.com/index.php/CM/

Research Article

# A Unified Nonlinear Mathematical Model Based on Smoking-Vaping Dynamics with Spectral Graph Analysis and Simulation

**Muhammad Sadaqat Talha[1], Muhammad Waseem[1], Zeeshan Ali[2], Nahid Fatima[3], Kamal Shah[3], Thabet Abdeljawad[3,4*]**

[1] Department of Mathematics, COMSATS University Islamabad, Vehari Campus, Pakistan
[2] Department of Information Management, National Yunlin University of Science and Technology, Douliou, Taiwan
[3] Department of Mathematics and Sciences, Prince Sultan University, Riyadh 11586, Saudi Arabia
[4] Department of Mathematics and Applied Mathematics, School of Science and Technology, Sefako Makgatho Health Sciences University, Ga-Rankuwa, South Africa
E-mail: tabdeljawad@psu.edu.sa

**Received:** 30 January 2026; **Revised:** 1 April 2026; **Accepted:** 9 April 2026

**Abstract:** This research presents a nonlinear mathematical approach that integrates smoking and vaping dynamics in a one population. The model is defined as a system of nonlinear ordinary differential equations and rigorously analyzed to provied the existence, uniqueness and boundedness of solutions. The disease-free and endemic equilibrium states are obtained to investigate the major dynamical characteristics of the disease as well as the basic reproduction number is obtained using the next-generation matrix method. Stability analyses encompassing both local and global perspectives are conducted to detail the threshold conditions and the future behavior of the system. To examine the structure and the interaction of the model diagonally, a signal flow graph is plotted and analyzed using spectral graph theory. The measures include graph energy and Estrada index, which are used to establish the connectivity of the network, the feedback and flow of information among the variables. Moreover, sensitivity analysis is conducted to indicate the key parameters which have the greatest influence on the transmission of smoking and vaping, thereby causing the control strategies to be developed. The numerical experiments confirm the analytical findings besides showing the strength of the suggested framework to represent the complex correlation between the behaviors of smoking and vaping accurately. The simulations were further supported by a MATLAB Simulink model that demonstrated the system equations as an animated block diagram which besides allowing the visual exploration of state transitions and parameter sensitivity in real-time also provides a user-friendly tool for scenario testing and educational demonstration.

***Keywords*:** smoking-vaping dynamics, nonlinear ordinary differential equations, basic reproduction number, spectral graph theory, mathematical epidemiology, infectious disease modeling

**MSC:** 34A34, 65P40, 68U20, 34K28, 65C20

## 1. Introduction

Smoking is still one of the top preventable causes of death, accounting for almost 7 million deaths every year all over the world. Out of the total, over 6 million deaths are among the puffs and about 0.9 million deaths are of non-smokers who


DOI: https://doi.org/10.37256/cm.7320269704

get exposed to tobacco smoke against their will [1]. The global smoking community, which is approximated at 1.1 billion people, is mostly found in low-income and middle-income nations, where the negative effects of tobacco usage are mostly public health and economic stability issues. The public health issue of smoking is that those who smoke will die sooner, resulting in not only loss of income of the family but also huge financial burdens due to increased healthcare costs and decreased workforce productivity. Tobacco consumption is the reason for economic losses of almost 2 trillion every year, which is equivalent to 2% of the world's gross domestic product. It is estimated that about 30% of these losses are due to the medical costs of treating the diseases caused by tobacco, while the remaining part comes from the decreased labor output and the productivity losses resulting from smoking-related death and diseases [2]. Smoking is the act of burning or heating substances and inhaling the resulting smoke through the mouth or nose into the lungs. The active ingredients in tobacco smoke get to the blood stream quickly through the lungs, and they are then taken to the brain, where their effects are felt physiologically. Tobacco products are the main ones people smokes and use worldwide, and more than 1.3 billion people are global smokers [3]. The act of smoking is a primary cause of many chronic diseases, which may be asymptomatic, e.g. lung cancer, diabetes, heart conditions and long-lasting respiratory disorders [4]. Besides that, smoking is still the main culprit in the case of many cancer types, e.g. the ones occurring in the mouth, throat, stomach, cervix, and even breast and pancreas cancers [5]. Nearly all the drinking of smoke health hazards can be traced back to the presence of more than 4000 chemical compounds and toxic substances that are in cigarette smoke, with many of them being classified as carcinogens and thus are a serious threat to human health [6, 7]. Recently, the debate on smoking-related health risks has been extended with the introduction of electronic cigarettes, which are regarded as a new way of delivering nicotine and are considered less harmful than regular tobacco. Nevertheless, there is a growing body of evidence that e-cigarette use also carries a number of adverse health effects [8, 9]. Research on the long-term consequences of e-cigarette consumption is still ongoing, but current investigations have noted both short and long term respiratory problems connected to vaping [10]. In the case of older smokers who switch to e-cigarettes to quit smoking, the potential health risks might not be such a big problem if the comparison is made with the heavy smoking that has already been done and well documented. On the other hand, the e-cigarette usage by teenagers and young adults is a much bigger public health problem, as the young start to smoke more, the kids will end up suffering the most in terms of health over the years. The younger generation usually experience respiratory problems as the first sign of health issues, and this has been connected to chronic bronchitis, asthma, and others that cause progressive lung function decline later in life [11]. Another issue related to this problem is the increasing number of people who use both traditional and e-cigarettes, which is referred to as dual use. The current studies about the health impacts of dual use are still inconclusive. While some researchers find harm reduction because of less smoking [12], others say that smoking with vaping leads to no health benefits at all. In some instances, dual users are at the same or even higher risk of health problems than people using only one type of product. What is significant is that the majority of existing studies consider smoking and vaping separately, and thus the interaction effects are still not well understood [13–17]. With the increasing shift from conventional tobacco smoking to the use of e-cigarettes as the main source of nicotine intake, Straughan [18] introduced a mathematical model capturing the interactions of non-smokers, tobacco smokers, and e-cigarette users, which was governed by peer pressure. The model shows several equilibrium positions whose stability analysis reveals the long-term dynamics of smoking behavior. To combat the heavy public health problem caused by smoking, Uçar et al. [19] introduced a new smoking model based on the Atangana-Baleanu fractional derivative with Mittag-Leffler kernel, thus proposing e-cigarette smoking model refill. Their research proves the existence and uniqueness of solutions and, in addition, through numerical simulations, shows how fractional-order effects can either slow down or hasten the transition between different smoking groups.

Researchers use compartmental models to study smoking and vaping because this method has strong roots in behavioral epidemiology which shows how people develop their habits and norms through processes that resemble disease transmission. The system defines behavior as a social process which people learn through their interactions with others and their ability to watch and experience peer pressure so it connects to social contagion theory and research about spreading disease through social networks [20–22]. People who experience social pressure to change their behavior between non-smoking and smoking and vaping use transition rates instead of biological incidence to show their movement between different behavioral states. The development of multiple mathematical models to describe how individual decisions interact with their social surroundings has its origins in this viewpoint.

Mathematical modeling is a very powerful and indispensable tool for analyzing the dynamics of complex diseases (smoking behavior, for instance), as well as for designing effective prevention measures that aim to reduce the spread of the disease. Such models through simulation-based analysis not only offer great insight into the long-term consequences of control strategies and intervention policies but also are a good method for their evaluation [23–26]. One of the basic models that have been widely used in the field of epidemiology is the compartmental model and particularly the classical Susceptible-Infected-Recovered (SIR) structure. This framework has been extended in numerous ways such as Susceptible-Exposed-Infected-Recovered (SEIR), Susceptible-Exposed-Infected-Recovered-Quarantined (SEIRQ), and similar models, which have been developed and applied to better capture the processes that govern disease transmission and the transition of people between different states. The rate at which individuals initiate or cease a behavior constitutes a critical element in modeling behavioral dynamics, as it determines the frequency of transitions between groups. Depending on the modeling objectives and assumptions, researchers have employed various functional forms to represent these rates, including bilinear, saturated, exponential, nonlinear, and fractional forms [27–32]. The developed models enable researchers to study three different phenomena which include how population groups exist in their communities how social contact limitations lead to complete contact establishment and how memory-based systems affect social behavior transformations. Building on these approaches, a range of mathematical models has been developed to represent smoking dynamics in diverse populations. Castillo-Garsow et al. introduced a Potential-Smokers-Quitters (PSQ) compartmental framework that divided the population into three behavioral categories, examining both linear and nonlinear rates of initiation and cessation [33]. In the following research, Sharomi et al. took the smoking model further by splitting former smokers into two categories, temporary and permanent quitters, to better describe the quitting and returning behaviors [34]. Recently, Alkhudhari et al. have re-evaluated these models and have studied the social and behavioral pressure effects on the temporary quitters in the smoking population [35]. Sofia et al. [36] and Numpanviwat and Pholuang [37] established positivity and boundedness of solutions, ensuring that model outcomes remain biologically and socially meaningful. The process of smoking cessation faces major obstacles because people who try to stop smoking often experience relapse according to research which used Sofia et al. models to show this effect on long-lasting patterns of behavior. Through these studies researchers established the basic reproduction number which they defined as the $\mathscr{R}_0$ threshold parameter. The smoking-free equilibrium remains stable when $\mathscr{R}_0 < 1$ because this condition leads to complete smoking behavior elimination, but $\mathscr{R}_0 > 1$ results in continuous smoking at endemic levels according to [38]. The later models built on earlier models to create more accurate smoking data because they added new elements to their operational framework. Noersena et al. developed a system which tracks users of traditional cigarettes and e-cigarettes separately to show how rapidly nicotine product alternatives have become popular according to their research results [39]. Demographic heterogeneity has also been incorporated, Bushnaq et al. [40] proposed an age-structured model to capture variations in smoking initiation and cessation across different age groups. Behavioral progression within smoking populations has been modeled in greater detail as well. Ansori [41] presented a discrete-time model distinguishing early-stage smokers from heavy, established smokers. Despite these substantial developments current research not only builds on but also develops an innovative nonlinear mathematical framework that is able to reveal the intertwined dynamics of smoking and vaping in one unified population, based on the presented smoking and e-cigarette models.

## 2. Novelty of the work

The present study introduces a number of original contributions that set it apart from the existing mathematical models of smoking and e-cigarette use. To begin with, a unified nonlinear population framework is constructed to simultaneously describe the linked dynamics of traditional smoking and vaping in a one system. Unlike previous studies, which have modeled smoking and e-cigarette use separately or have treated one behavior as a minor extension of the other, this research explicitly depicts their interaction and coexistence, thus giving a more realistic view of the current smoking practices. Moreover, the new model is subjected to a thorough theoretical analysis. Basic mathematical properties such as the existence, uniqueness, and boundedness of solutions are verified, thus assuring the well-posedness of the system. The computation of the basic reproduction number using the next-generation matrix method, together with local and

global stability analyses of the disease-free equilibrium, provides specific threshold conditions regulating the persistence or extinction of smoking and vaping habits. Third, a novel structural analysis is introduced by the construction of a signal flow graph related to the model. This study, through the utilization of spectral graph measures like graph energy and the Estrada index, grants novel quantitative insights into the global connectivity, the feedback strength, and the information flow amongst the state variables. The spectral characterization of the smoking-vaping dynamics has not been investigated in this manner before and thus adds a network-based interpretation to the traditional compartmental modeling approach. Finally, the sensitivity analysis is integrated in this spectral-dynamical framework to point out the most influential parameters that are responsible for the transmission of smoking and vaping. Not only does this combined analytical approach improve the interpretability, but it also aids the development of the control and intervention strategies effective. Consequently, the proposed framework represents an advance in the existing literature by amalgamating the nonlinear dynamics, the spectral graph theory, and the stability analysis into a single integrated model for understanding smoking and vaping interactions. The model further gets implemented in MATLAB Simulink to facilitate the interactive simulation, and parameter exploration thereby providing a visual platform that is accessible, for scenario analysis, and educational applications in public health. Overall, the proposed framework advances the current literature by unifying nonlinear dynamics, spectral graph theory, stability analysis, and interactive computational implementation into a single coherent model for understanding smoking and vaping interactions.

## 3. Model formulation

The presented model provides an analysis of cigarette consumption behavior, which is represented by layering the entire population, $N(t)$, into six separate groups: Potential smokers $P_S(t)$, Occasional smokers $O_S(t)$, Regular smokers $R_S(t)$, Vapers $V_E(t)$, Temporarily Quit smokers $Q_T(t)$ and Permanently Quit smokers $Q_P(t)$. The transitions of people among these compartments are controlled by a set of interconnected ordinary differential equations, which have as parameters the rates of different social, behavioral, and biological transitions.

• **Dynamics of Potential Smokers** $(P_S)$

The rate of change of the Potential Users compartment $\frac{dP_S}{dt}$, is characterized by one inflow and three outflows. The single inflow is the recruitment rate $+\lambda$, which represents a constant stream of new individuals entering the susceptible population, for instance, through birth or immigration. The first outflow $-\beta P_S R_S$, models the initiation of smoking through social contact. Based on the principle of mass action, its rate is proportional to the product of the Potential smokers ($P_S$) and Regular smoker ($R_S$) populations with $\beta$ being the effective contact rate that leads to Occasional smoking. The second outflow $-\beta_v P_S V_E$, similarly models the initiation of vaping, where the rate is proportional to the interactions between Potential users ($P_S$) and Vapers ($V_E$), governed by the vaping contact rate $\beta_v$. The final outflow $-\eta P_S$, accounts for the removal of individuals from the compartment due to natural death, where $\eta$ is the per-capita natural death rate assumed to be constant across all compartments.

$$\frac{dP_S}{dt} = \lambda - \beta P_S R_S - \beta_v P_S V_E - \eta P_S.$$

• **Dynamics of Occasional smokers** $(O_S)$

The Occasional smokers compartment $\frac{dO_S}{dt}$, serves as a transitional state. Its population is fed by a single inflow $+\beta P_S R_S$, which directly corresponds to the individuals who have just initiated smoking from the Potential smokers pool. There are two outflows. The first $-\alpha_1 O_S$, represents the progression from experimental use to habitual, addicted smoking. This transition occurs at a per-capita rate of $\alpha_1$, moving these individuals into the Regular smoker ($R_S$) compartment. The second outflow is the standard natural death term $-\eta O_S$.

$$\frac{dO_S}{dt} = \beta P_S R_S - \alpha_1 O_S - \eta O_S.$$

• **Dynamics of Regular smokers** $(R_S)$

The rate of change for the core Smoker population $\frac{dR_S}{dt}$, is determined by three inflows and three outflows. The first inflow $+\alpha_1 O$, is the stream of individuals who have progressed from being Occasional smokers. The second inflow $+\alpha_2 R_S Q_T$, models relapse. This mass-action term indicates that the rate of relapse is proportional to the interactions between Temporarily Quit users $(Q_T)$ and current smokers $(R_S)$ with $\alpha_2$ as the effective contact rate causing relapse. The third inflow $+\alpha_v V_E$, represents the gateway effect, where Vapers transition to become regular Smokers at a per-capita rate of $\alpha_v$. The outflows are grouped into $-(\gamma+\varepsilon)R_S$ and a death term. The term $-\gamma R_S$ represents smokers who attempt to quit nicotine at a per-capita rate $\gamma$. The term $-\varepsilon R_S$ captures smokers who switch to vaping as a harm reduction strategy or cessation aid, at a per-capita rate $\varepsilon$. The final outflow is natural mortality $-\eta R_S$.

$$\frac{dR_S}{dt} = \alpha_1 O_S + \alpha_2 R_S Q_T + \alpha_v V_E - (\gamma+\varepsilon)R_S - \eta R_S.$$

• **Dynamics of Vapers** $(V_E)$

The Vapers compartment $\frac{dV_E}{dt}$, is a central hub with dynamic flows. It gains population from two sources. The first inflow $+\beta_v P_S V_E$, represents the direct initiation of vaping by Potential users influenced by current Vapers. The second inflow $+\varepsilon R_S$, consists of former Smokers who have switched to e-cigarettes. There are three outflows. The first $-\alpha_v V_E$, is the gateway transition to regular smoking as previously described. The second $-\theta V_E$, represents Vapers who attempt to quit nicotine use entirely, moving to the Temporarily-Quit $(Q_T)$ compartment at a per-capita rate $\theta$. The third outflow is the natural death term $-\eta V_E$.

$$\frac{dV_E}{dt} = \beta_v P_S V_E + \varepsilon R_S - (\alpha_v + \theta + \eta)V_E.$$

• **Dynamics of Temporarily-Quit smokers ($Q_T$)**

The Temporarily Quit users compartment $\frac{dQ_T}{dt}$, is a state of high relapse risk. The first inflow $+\gamma(1-\delta)R_S$, represents the fraction of smokers who attempt to quit (at rate $\gamma$) but do not achieve permanent cessation. Here $\delta$ is the fraction that succeeds permanently, so $(1-\delta)$ is the fraction that enters this temporary state. The second inflow $+\theta V_E$, is comprised of Vapers who have ceased nicotine use. The primary outflow is relapse $-\alpha_2 R_S Q_T$, sending individuals back to the Smoker compartment upon effective contact with smokers. The other outflow is natural death $-\eta Q_T$.

$$\frac{dQ_T}{dt} = \gamma(1-\delta)R_S + \theta V_E - \alpha_2 R_S Q_T - \eta Q_T.$$

• **Dynamics of Permanently-Quit smokers ($Q_P$)**

The equation for the Permanently Quit users $\frac{dQ_P}{dt}$, describes the most stable recovered state. The sole influx into this compartment is $+\delta\gamma R_S$. This term represents the fraction $\delta$ of the total smokers attempting to quit $(\gamma R_S)$ who are successful in achieving long-term abstinence. This is an absorbing state in terms of behavior, meaning the only way to leave this compartment is through the natural death outflow, $-\eta Q_P$.

$$\frac{dQ_P}{dt} = \delta\gamma R_S - \eta Q_P.$$

Graphic illustrations of the proposed smoking model can be seen in the following Figure 1, which visually demonstrate the model structure, interactions among compartments and the overall dynamical behavior of the system (1).

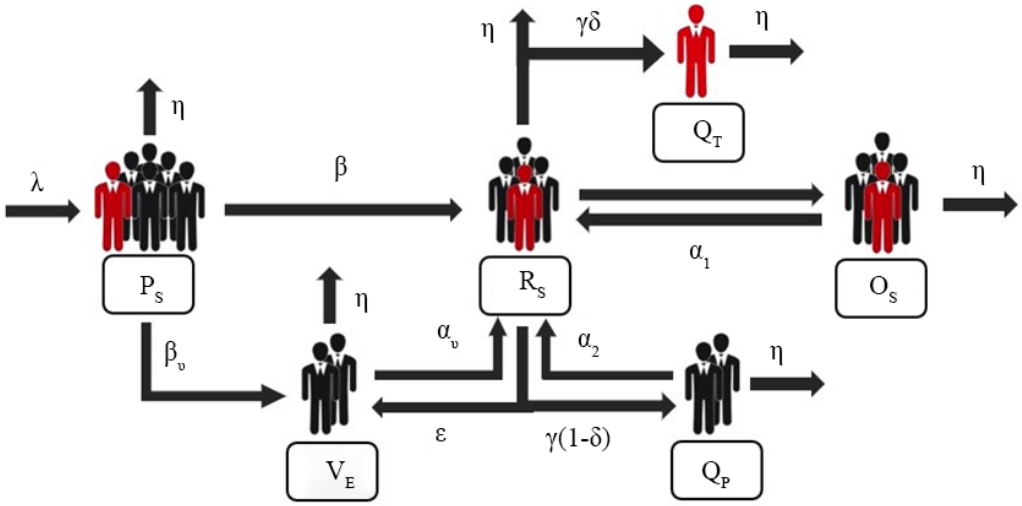


**Figure 1.** Graphic illustrations of the smoking model

These dynamic flows are precisely modeled by the following system of differential equations:

$$\begin{aligned}
\frac{dP_S}{dt} &= \lambda - \beta P_S R_S - \beta_v P_S V_E - \eta P_S,\\
\frac{dO_S}{dt} &= \beta P_S R_S - (\alpha_1 + \eta) O_S,\\
\frac{dR_S}{dt} &= \alpha_1 O_S + \alpha_2 R_S Q_T + \alpha_v V_E - (\gamma + \varepsilon + \eta) R_S,\\
\frac{dV_E}{dt} &= \beta_v P_S V_E + \varepsilon R_S - (\alpha_v + \theta + \eta) V_E,\\
\frac{dQ_T}{dt} &= \gamma(1-\delta) R_S + \theta V_E - \alpha_2 R_S Q_T - \eta Q_T,\\
\frac{dQ_P}{dt} &= \delta\gamma R_S - \eta Q_P.
\end{aligned} \tag{1}$$

The model described above incorporates demographic turnover explicitly via a recruitment term $\lambda$ and a natural death rate $\eta$, which together ensure that the total population evolves according to $\frac{dN}{dt} = \lambda - \eta N$. Although the mathematical structure makes use of terms resembling mass-action kinetics, these are intended to capture social contagion mechanisms, individuals shift between behavioral states under the influence of peer interactions and prevailing social norms.

## 4. Mathematical analysis of the model

This section discusses the existence and uniqueness, positivity, boundedness, equilibria and basic reproduction number of the proposed smoking model (1).

### 4.1 *Existence and uniqueness*

**Theorem 1** The system has a unique solution for all $t$ starting from the initial conditions $P_S(0) > 0$, $O_S(0) \geq 0$, $R_S(0) \geq 0$, $V_E(0) \geq 0$, $Q_T(0) \geq 0$, $Q_P(0) \geq 0$ which allows the system to remain in the state space of $C(\mathbb{R}^+, \mathbb{R}^6_+)$ for all time $t$ greater than or equal to zero.

**Proof.** The model system transforms into $\dot{y} = g(y)$ which describes its behavior through this equation:

$$\dot{y} = \begin{pmatrix} \dot{P}_S \\ \dot{O}_S \\ \dot{R}_S \\ \dot{V}_E \\ \dot{Q}_T \\ \dot{Q}_P \end{pmatrix} = \begin{pmatrix} \lambda - \beta P_S R_S - \beta_v P_S V_E - \eta P_S \\ \beta P_S R_S - (\alpha_1 + \eta) O_S \\ \alpha_1 O_S + \alpha_2 R_S Q_T + \alpha_v V_E - (\gamma + \varepsilon + \eta) R_S \\ \beta_v P_S V_E + \varepsilon R_S - (\alpha_v + \theta + \eta) V_E \\ \gamma(1-\delta) R_S + \theta V_E - \alpha_2 R_S Q_T - \eta Q_T \\ \delta \gamma R_S - \eta Q_P \end{pmatrix}$$

The vector field $g(x)$ consists of three components which maintain continuous differentiability throughout most of the space $C(\mathbb{R}_+, \mathbb{R}^6_+)$, making it possible to establish that $g \in C^1$ space which results in $g$ demonstrating local Lipschitz continuity. The system of differential equations has one specific local solution according to the fundamental existence and uniqueness theorem [42].

$$y(t) \in \mathbb{R}^6_+, \quad \forall t \geq 0$$

The model requires non-negative solutions at every time point which will be proved in the upcoming theorem because it models population dynamics. □

**Theorem 2** The region $\Omega_+ = \{(P_S, O_S, R_S, V_E, Q_T, Q_P) \in \mathbb{R}^6_+ \,|\, P_S(0) > 0, O_S(0) \geq 0, R_S(0) \geq 0, V_E(0) \geq 0, Q_T(0) \geq 0, Q_P(0) \geq 0\}$ is positively invariant for the model (1).

**Proof.** Consider the potential smoker compartment:

$$\frac{dP_S}{dt} = \lambda - \beta P_S R_S - \beta_v P_S V_E - \eta P_S \geq -(\beta R_S + \beta_v V_E + \eta) P_S.$$

Separating variables and integrating:

$$\int_{P_S(0)}^{P_S(t)} \frac{dP_S}{P_S} \geq -\int_0^t (\beta R_S(u) + \beta_v V_E(u) + \eta) du,$$

$$P_S(t) \geq P_S(0) \exp\left(-\int_0^t (\beta R_S(u) + \beta_v V_E(u) + \eta) du\right) > 0.$$

Similarly for other compartments:

$$O_S(t) \geq O_S(0)e^{-(\alpha_1+\eta)t} \geq 0$$

$$R_S(t) \geq S_S(0)e^{-[(\gamma+\varepsilon)+\eta]t} \geq 0$$

$$V_E(t) \geq V_E(0)e^{-(\alpha_v+\theta+\eta)t} \geq 0$$

$$Q_T(t) \geq Q_T(0)e^{-(\alpha_2 R_S+\eta)t} \geq 0$$

$$Q_P(t) \geq Q_P(0)e^{-\eta t} \geq 0.$$

Thus, $\Omega_+$ is positively invariant. Then the solutions $P_S(0) > 0$, $O_S(0) \geq 0$, $R_S(0) \geq 0$, $V_E(0) \geq 0$, $Q_T(0) \geq 0$, $Q_P(0) \geq 0$ of the model are positive for all $t > 0$. □

## 4.2 *Boundedness of solutions*

In this subsection, model boundedness is discussed. Utilize theorem below to obtain feasible region for this smoking model (1).

**Theorem 3** The set of feasible solutions $\Omega \subset \mathbb{R}^6$ with initial conditions $P_S(0) > 0$, $O_S(0) \geq 0$, $R_S(0) \geq 0$, $V_E(0) \geq 0$, $Q_T(0) \geq 0$, $Q_P(0) \geq 0$ creates a positive invariant set which ensures that all starting points within this set will stay in biologically valid areas throughout time.

**Proof.** Define the total population function as:

$$N_{SV}(t) = P_S(t) + O_S(t) + R_S(t) + V_E(t) + Q_T(t) + Q_P(t).$$

Differentiating $N_{SV}(t)$ with respect to time gives

$$\frac{dN_{SV}}{dt} = \frac{dP_S}{dt} + \frac{dO_S}{dt} + \frac{dR_S}{dt} + \frac{dV_E}{dt} + \frac{dQ_T}{dt} + \frac{dQ_P}{dt}.$$

By summing the governing equations of the model, all internal transfer terms cancel, and we obtain

$$\frac{dN_{SV}}{dt} = \lambda - \eta N_{SV},$$

where $\lambda > 0$ denotes the recruitment rate and $\eta > 0$ represents the natural removal rate. The above equation is a first-order linear ordinary differential equation. Separating variables yields

$$\frac{dN_{SV}}{\lambda - \eta N_{SV}} = dt.$$

Integrating both sides, we have

$$\int_{N_{SV}(0)}^{N_{SV}(t)} \frac{dN_{SV}}{\lambda - \eta N_{SV}} = \int_0^t dt.$$

This gives

$$-\frac{1}{\eta}\ln\big(\lambda - \eta N_{SV}(t)\big) + \frac{1}{\eta}\ln\big(\lambda - \eta N_{SV}(0)\big) = t.$$

Solving for $N_{SV}(t)$, we obtain

$$N_{SV}(t) = \frac{\lambda}{\eta} + \left(N_{SV}(0) - \frac{\lambda}{\eta}\right) e^{-\eta t}.$$

Since $N_{SV}(0) \geq 0$, it follows that $N_{SV}(t) \geq 0$ for all $t > 0$. Moreover,

$$\lim_{t\to\infty} N_{SV}(t) = \frac{\lambda}{\eta},$$

which implies that the total population remains bounded. Therefore, the feasible region

$$\Omega = \left\{ (P_S, O_S, R_S, V_E, Q_T, Q_P) \in \mathbb{R}_+^6 \;\middle|\; 0 \leq N_{SV}(t) \leq \frac{\lambda}{\eta} \right\}$$

is positively invariant. Hence, all solution trajectories initiating in $\Omega$ remain in $\Omega$ for all $t > 0$, completing the proof. □

## 5. Analysis of the model

In this section, we first derive the disease-free equilibrium point of the proposed model and compute the associated basic reproduction number. We first determine local stability of the disease-free equilibrium through eigenvalue analysis of the Jacobian matrix which following that step leads to global stability proof through suitable Lyapunov-based methods.

### 5.1 *Disease-Free Equilibrium (DFE)*

**Theorem 4** The disease-free equilibrium $E_0$ occurs when $O_S = R_S = V_E = Q_T = Q_P = 0$ and is given by:

$$E_0 = \left(\frac{\lambda}{\eta}, 0, 0, 0, 0, 0\right).$$

### 5.2 *Basic reproduction number*

$R_0$ is the number of smoking-vaping cases that one smoker-vaper causes over the infectious period [43].

**Theorem 5** The basic reproduction number $R_0$ for the smoking model is:

$$R_0 = \frac{\lambda}{\eta(\gamma+\varepsilon+\eta)}\left(\frac{\beta\,\alpha_1}{\alpha_1+\eta}+\frac{\beta_v\,\varepsilon}{\alpha_v+\theta+\eta}\right).$$

**Proof.** By using the next generation matrix method, we consider the infected compartments $O_S$, $R_S$ and $V_E$. The new infections matrix $F$ and the transition matrix $V$ are:

$$F = \begin{pmatrix} \beta P_S R_S + \beta_v P_S V_E \\ 0 \\ 0 \end{pmatrix}, \quad V = \begin{pmatrix} \alpha_1 O_S + \eta O_S \\ -\alpha_1 O_S - \alpha_2 R_S Q_T - \alpha_v V_E + (\gamma+\varepsilon+\eta)R_S \\ -\beta_v P_S V_E - \varepsilon R_S + (\alpha_v+\theta+\eta)V_E \end{pmatrix}.$$

At disease-free equilibrium $P_{S0} = \frac{\lambda}{\eta}$, the Jacobian matrices are:

$$\mathscr{F} = \begin{pmatrix} 0 & \beta P_{S0} & \beta_v P_{S0} \\ 0 & 0 & 0 \\ 0 & 0 & 0 \end{pmatrix}, \quad \mathscr{V} = \begin{pmatrix} \alpha_1+\eta & 0 & 0 \\ -\alpha_1 & \gamma+\varepsilon+\eta & -\alpha_v \\ 0 & -\varepsilon & \alpha_v+\theta+\eta \end{pmatrix}.$$

The next generation matrix is $\mathscr{F}\mathscr{V}^{-1}$. The spectral radius gives:

$$R_0 = \rho(\mathscr{F}\mathscr{V}^{-1}) = \frac{\beta\lambda}{\eta(\alpha_1+\eta)}\cdot\frac{\alpha_1}{\gamma+\varepsilon+\eta} + \frac{\beta_v\lambda}{\eta(\alpha_v+\theta+\eta)}\cdot\frac{\varepsilon}{\gamma+\varepsilon+\eta}$$

$$R_0 = \mathscr{F}\mathscr{V}^{-1} = \frac{\beta\lambda\alpha_1}{\eta(\alpha_1+\eta)(\gamma+\varepsilon+\eta)} + \frac{\beta_v\lambda\varepsilon}{\eta(\alpha_v+\theta+\eta)(\gamma+\varepsilon+\eta)}$$

$$R_0 = \frac{\lambda}{\eta(\gamma+\varepsilon+\eta)}\left(\frac{\beta\,\alpha_1}{\alpha_1+\eta}+\frac{\beta_v\,\varepsilon}{\alpha_v+\theta+\eta}\right).$$

□

## 5.3 *Endemic equilibrium*

The endemic equilibrium shows that smoking and vaping will continue in the population without elimination throughout time. The endemic equilibrium shows continuous transmission of smoking because the transmission rate $R_0 > 1$. The endemic point is established when all state variables which include potential smokers, occasional smokers, regular smokers, vapers, quitters and permanent quitters are nonzero at equilibrium $(P_S^*, O_S^*, R_S^*, V_E^*, Q_T^*, Q_P^*) \neq (0,0,0,0,0,0)$ and by setting the right hand side of the proposed system equal to zero.

**Theorem 6** The system of equations has a unique positive endemic equilibrium point $E^* = (P_S^*, O_S^*, R_S^*, V_E^*, Q_T^*, Q_P^*)$ if and only if the basic reproduction number $R_0 > 1$.

**Proof.** If $R_0 > 1$, then the system possesses a nonnegative endemic equilibrium $E^* \neq (0,0,0,0,0,0)$, obtained by setting the system equations to zero, with components given by:

$$P_S^* = \frac{\lambda}{\beta R_S^* + \beta_v V_E^* + \eta},$$

$$O_S^* = \frac{\beta P_S^* R_S^*}{\alpha_1 + \eta},$$

$$R_S^* = \frac{\alpha_1 O_S^* + \alpha_2 R_S^* Q_T^* + \alpha_v V_E^*}{\gamma + \varepsilon + \eta},$$

$$V_E^* = \frac{\beta_v P_S^* V_E^* + \varepsilon R_S^*}{\alpha_v + \theta + \eta},$$

$$Q_T^* = \frac{\gamma(1-\delta) R_S^* + \theta V_E^*}{\alpha_2 R_S^* + \eta},$$

$$Q_P^* = \frac{\delta \gamma R_S^*}{\eta}.$$

□

## 5.4 *Local stability*

We will investigate both the local stability and global stability of the proposed dynamical system using analytical techniques like those advanced in [44].

## 5.5 *Local stability of the Disease-Free Equilibrium (DFE)*

**Theorem 7** The disease-free equilibrium $E_0$ is locally asymptotically stable when $R_0 < 1$ and unstable when $R_0 > 1$.

**Proof.** The Jacobian matrix at DFE is:

$$J_{E_0} = \begin{pmatrix} -\eta & 0 & -\beta P_{S0} & -\beta_v P_{S0} & 0 & 0 \\ 0 & -(\alpha_1 + \eta) & \beta P_{S0} & 0 & 0 & 0 \\ 0 & \alpha_1 & -(\gamma + \varepsilon + \eta) & \alpha_v & \alpha_2 R_{S0} & 0 \\ 0 & 0 & \varepsilon & -(\alpha_v + \theta + \eta) & 0 & 0 \\ 0 & 0 & \gamma(1-\delta) & \theta & -(\alpha_2 R_{S0} + \eta) & 0 \\ 0 & 0 & \delta\gamma & 0 & 0 & -\eta \end{pmatrix}$$

where $P_{S0} = \frac{\lambda}{\eta}$. The eigenvalues of the Jacobian at the disease-free equilibrium $E_0$ can be summarized as follows:

$$\lambda_1 = \lambda_2 = \lambda_3 = -\eta.$$

$$\lambda_4 = -(\gamma + \varepsilon + \eta).$$

From the quadratic equation

$$(\lambda+\alpha_1+\eta)(\lambda+\alpha_v+\theta+\eta)-(\alpha_1+\eta)(\alpha_v+\theta+\eta)R_0=0,$$

we obtain

$$\lambda_{5,6}=\frac{-\left[(\alpha_1+\eta)+(\alpha_v+\theta+\eta)\right]\pm\sqrt{\left[(\alpha_1+\eta)-(\alpha_v+\theta+\eta)\right]^2+4(\alpha_1+\eta)(\alpha_v+\theta+\eta)(R_0-1)}}{2}.$$

The characteristic equation of the Jacobian matrix $J_{E_0}$ is given by

$$(\lambda+\eta)^3(\lambda+\gamma+\varepsilon+\eta)\Big[(\lambda+\alpha_1+\eta)(\lambda+\alpha_v+\theta+\eta)-(\alpha_1+\eta)(\alpha_v+\theta+\eta)R_0\Big]=0.$$

All eigenvalues have negative real parts when $R_0<1$. The system demonstrates local asymptotic stability because all eigenvalues of the Jacobian matrix exhibit negative real parts, which meet the Routh-Hurwitz stability criterion requirements. □

## 5.6 *Global stability*

**Theorem 8** The Disease-Free Equilibrium (DFE) $E_0$ of the system is Globally Asymptotically Stable (GAS) inside the invariant set $\Omega$ if the basic reproduction number $R_0\leq 1$, and unstable if $R_0>1$.

**Proof.** We prove the Global Asymptotic Stability (GAS) of the Disease-Free Equilibrium (DFE) $E_0$ using a Lyapunov function and LaSalle's invariance principle. Consider the candidate Lyapunov function

$$\mathscr{L}(P_S,O_S,R_S,V_E,Q_T,Q_P)=\frac{P_S-P_{S0}-P_{S0}\ln\frac{P_S}{P_{S0}}}{P_{S0}}+\frac{V_E-V_{E0}-V_{E0}\ln\frac{V_E}{V_{E0}}}{V_{E0}},$$

where $P_{S0}=\frac{\lambda}{\eta}$ and $V_{E0}=0$ at the DFE. This function is non-negative and $\mathscr{L}=0$ if and only if $(P_S,V_E)=(P_{S0},V_{E0})$. Differentiating $\mathscr{L}$ with respect to time:

$$\frac{d\mathscr{L}}{dt}\leq\frac{P_S-P_{S0}}{P_S}\frac{dP_S}{dt}+\frac{V_E-V_{E0}}{V}\frac{dV_E}{dt},$$

and substituting the system dynamics:

$$\frac{dP_S}{dt}=\lambda-(\beta R_S+\beta_v V_E+\eta)P_S,\quad \frac{dV_E}{dt}=\beta_v P_S V_E+\varepsilon R_S-(\alpha_v+\theta+\eta)V_E,$$

we get

$$\frac{d\mathscr{L}}{dt}\leq\frac{P_S-P_{S0}}{P_S}\left(\lambda-(\beta R_S+\beta_v V_E+\eta)P_S\right)+\frac{V_E-V_{E0}}{V_E}\left(\beta_v P_S V_E+\varepsilon R_S-(\alpha_v+\theta+\eta)V_E\right).$$

Using $P_{S0} = \frac{\lambda}{\eta}$ and $V_{E0} = 0$, we have

$$\frac{d\mathscr{L}}{dt} \leq -\frac{\eta}{P_{S0}}(P_S - P_{S0})^2 - \frac{\varepsilon}{V_{E0}}(V_E - V_{E0})^2 \leq 0.$$

Hence, $\frac{d\mathscr{L}}{dt} \leq 0$ for all $(P_S, O_S, R_S, V_E, Q_T, Q_P) \in \Omega$.
By LaSalle's invariance principle, since $\mathscr{L} \geq 0$ and $\frac{d\mathscr{L}}{dt} \leq 0$ with equality only at $E_0$, it follows that

$$E_0 \text{ is globally asymptotically stable in } \Omega \text{ if } R_0 \leq 1.$$

Conversely if $R_0 > 1$, there exists at least one positive eigenvalue in the Jacobian at $E_0$, implying that $E_0$ is unstable. □

**Theorem 9** The endemic equilibrium $E^* = (P_S^*, O_S^*, R_S^*, V_E^*, Q_T^*, Q_P^*)$ of the system is Globally Asymptotically Stable (GAS) within the feasible region $\Gamma$ when $\mathscr{R}_0 > 1$. If $\mathscr{R}_0 \leq 1$, the endemic equilibrium is not feasible or becomes unstable.

**Proof.** We establish the global asymptotic stability of $E^*$ by constructing a Lyapunov function and applying LaSalle's invariance principle. Consider the candidate function:

$$\mathscr{V}(P_S, O_S, R_S, V_E, Q_T, Q_P) = \sum_{X \in \mathscr{M}} \left( X - X^* - X^* \ln \frac{X}{X^*} \right),$$

where $\mathscr{M} = \{P_S, O_S, R_S, V_E, Q_T, Q_P\}$. For each $X > 0$, the function $X - X^* - X^* \ln(X/X^*)$ is nonnegative and equals zero if and only if $X = X^*$. Hence $\mathscr{V}$ is positive definite on $\Gamma$ and vanishes only at $E^*$. The time derivative of $\mathscr{V}$ along solutions of the system is

$$\frac{d\mathscr{V}}{dt} = \sum_{X \in \mathscr{M}} \left( 1 - \frac{X^*}{X} \right) \frac{dX}{dt}.$$

We now substitute the model equations. The dynamics are given by:

$$\frac{dP_S}{dt} = \lambda - \beta P_S R_S - \beta_v P_S V_E - \eta P_S,$$

$$\frac{dO_S}{dt} = \beta P_S R_S - (\alpha_1 + \eta) O_S,$$

$$\frac{dR_S}{dt} = \alpha_1 O_S + \alpha_2 R_S Q_T + \alpha_v V_E - (\gamma + \varepsilon + \eta) R_S,$$

$$\frac{dV_E}{dt} = \beta_v P_S V_E + \varepsilon R_S - (\alpha_v + \theta + \eta) V_E,$$

$$\frac{dQ_T}{dt} = \gamma(1 - \delta) R_S + \theta V_E - \alpha_2 R_S Q_T - \eta Q_T,$$

$$\frac{dQ_P}{dt} = \delta\gamma R_S - \eta Q_P.$$

At the endemic equilibrium $E^*$, the following balance relations hold:

$$\lambda = \beta P_S^* R_S^* + \beta_v P_S^* V_E^* + \eta P_S^*, \tag{2}$$

$$\beta P_S^* R_S^* = (\alpha_1 + \eta) O_S^*, \tag{3}$$

$$\alpha_1 O_S^* + \alpha_2 R_S^* Q_T^* + \alpha_v V_E^* = (\gamma + \varepsilon + \eta) R_S^*, \tag{4}$$

$$\beta_v P_S^* V_E^* + \varepsilon R_S^* = (\alpha_v + \theta + \eta) V_E^*, \tag{5}$$

$$\gamma(1-\delta) R_S^* + \theta V_E^* = \alpha_2 R_S^* Q_T^* + \eta Q_T^*, \tag{6}$$

$$\delta\gamma R_S^* = \eta Q_P^*. \tag{7}$$

Substituting the derivatives and the equilibrium relations yields:

$$\begin{aligned}
\frac{d\mathscr{V}}{dt} = &\left(1 - \frac{P_S^*}{P_S}\right)\left[\beta P_S^* R_S^* + \beta_v P_S^* V_E^* + \eta P_S^* - \beta P_S R_S - \beta_v P_S V_E - \eta P_S\right] \\
&+ \left(1 - \frac{O_S^*}{O_S}\right)\left[\beta P_S R_S - (\alpha_1 + \eta) O_S\right] \\
&+ \left(1 - \frac{R_S^*}{R_S}\right)\left[\alpha_1 O_S + \alpha_2 R_S Q_T + \alpha_v V_E - (\gamma + \varepsilon + \eta) R_S\right] \\
&+ \left(1 - \frac{V_E^*}{V_E}\right)\left[\beta_v P_S V_E + \varepsilon R_S - (\alpha_v + \theta + \eta) V_E\right] \\
&+ \left(1 - \frac{Q_T^*}{Q_T}\right)\left[\gamma(1-\delta) R_S + \theta V_E - \alpha_2 R_S Q_T - \eta Q_T\right] \\
&+ \left(1 - \frac{Q_P^*}{Q_P}\right)\left[\delta\gamma R_S - \eta Q_P\right].
\end{aligned}$$

We now reorganize the terms using the equilibrium identities. For clarity, we define the following nonnegative functions:

$$\Phi_1 = \beta P_S^* R_S^* \left(2 - \frac{P_S^*}{P_S} - \frac{P_S R_S}{P_S^* R_S^*} \frac{O_S^*}{O_S}\right), \qquad \Phi_2 = \beta_v P_S^* V_E^* \left(2 - \frac{P_S^*}{P_S} - \frac{P_S V_E}{P_S^* V_E^*} \frac{V_E^*}{V_E}\right)$$

$$\Phi_3 = \alpha_1 O_S^* \left(2 - \frac{O_S^*}{O_S} - \frac{O_S R_S^*}{O_S^* R_S}\right), \qquad \Phi_4 = \alpha_v V_E^* \left(2 - \frac{V_E^*}{V_E} - \frac{V_E R_S^*}{V_E^* R_S}\right)$$

$$\Phi_5 = \varepsilon R_S^* \left(2 - \frac{R_S^*}{R_S} - \frac{R_S V_E^*}{R_S^* V_E}\right), \qquad \Phi_6 = \alpha_2 R_S^* Q_T^* \left(2 - \frac{Q_T^*}{Q_T} - \frac{R_S Q_T}{R_S^* Q_T^*} \frac{R_S^*}{R_S}\right)$$

$$\Phi_7 = \gamma(1-\delta) R_S^* \left(2 - \frac{R_S^*}{R_S} - \frac{R_S Q_T^*}{R_S^* Q_T}\right), \qquad \Phi_8 = \theta V_E^* \left(2 - \frac{V_E^*}{V_E} - \frac{V_E Q_T^*}{V_E^* Q_T}\right)$$

$$\Phi_9 = \eta P_S^* \left(2 - \frac{P_S^*}{P_S} - \frac{P_S}{P_S^*}\right), \qquad \Phi_{10} = \eta O_S^* \left(2 - \frac{O_S^*}{O_S} - \frac{O_S}{O_S^*}\right)$$

$$\Phi_{11} = \eta R_S^* \left(2 - \frac{R_S^*}{R_S} - \frac{R_S}{R_S^*}\right), \qquad \Phi_{12} = \eta V_E^* \left(2 - \frac{V_E^*}{V_E} - \frac{V_E}{V_E^*}\right)$$

$$\Phi_{13} = \eta Q_T^* \left(2 - \frac{Q_T^*}{Q_T} - \frac{Q_T}{Q_T^*}\right), \qquad \Phi_{14} = \eta Q_P^* \left(2 - \frac{Q_P^*}{Q_P} - \frac{Q_P}{Q_P^*}\right).$$

Each $\Phi_i$ is of the form $A(2-u-1/u)$ with $A \geq 0$ and $u > 0$, and satisfies $2-u-1/u \leq 0$ by the arithmetic–geometric mean inequality, with equality iff $u = 1$. Collecting terms, the derivative simplifies to

$$\frac{d\mathscr{V}}{dt} = -\sum_{i=1}^{14} \Phi_i \leq 0,$$

for all $(P_S, O_S, R_S, V_E, Q_T, Q_P) \in \Gamma$. Thus $\dot{\mathscr{V}}$ is negative semidefinite. We now determine the largest invariant set contained in $\mathscr{S} = \{(P_S, O_S, R_S, V_E, Q_T, Q_P) \in \Gamma : \dot{\mathscr{V}} = 0\}$. From the expressions above, $\dot{\mathscr{V}} = 0$ implies each $\Phi_i = 0$, which in turn forces:

$$\frac{P_S}{P_S^*} = 1, \quad \frac{O_S}{O_S^*} = 1, \quad \frac{R_S}{R_S^*} = 1, \quad \frac{V_E}{V_E^*} = 1, \quad \frac{Q_T}{Q_T^*} = 1, \quad \frac{Q_P}{Q_P^*} = 1.$$

Hence $\mathscr{S}$ consists only of the equilibrium point $E^*$. By LaSalle's invariance principle, every solution of the system starting in $\Gamma$ approaches $E^*$ as $t \to \infty$. Therefore $E^*$ is globally asymptotically stable whenever $\mathscr{R}_0 > 1$ and a positive endemic equilibrium exists. □

## 6. Signal flow graph and spectral characterization

The signal flow graph associated with the dynamical system $\vec{G}$ is shown in Figure 2 and is constructed directly from the governing equations given in (1). In this representation, each vertex corresponds to a state variable of the model, while a directed edge from one vertex to another vertex is introduced whenever the state variable has a direct influence on the evolution of another state variable , as illustrated by arrows connecting these quantities. The system demonstrates directional information transfer because of its construction which enables the system to show graph-theoretic model dynamics that demonstrate how key variables interact through causal pathways and feedback loops. The reader can find full theoretical information about signal flow graphs and their spectral properties in the sources [45, 46].

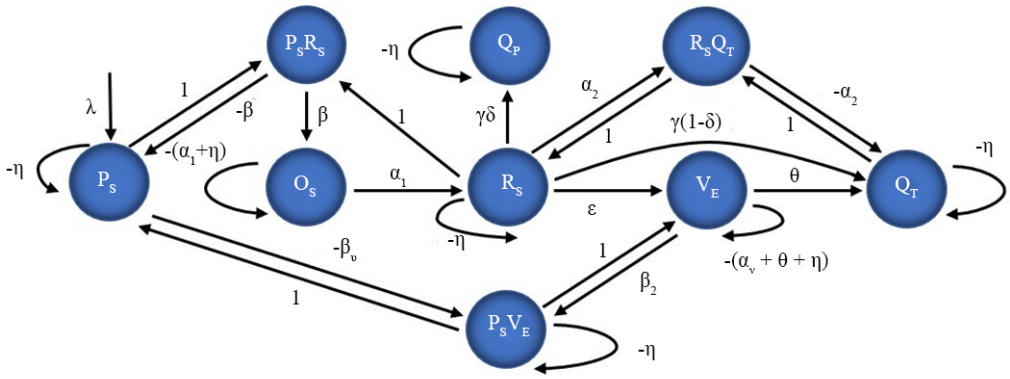


**Figure 2.** The signal flow graph of the smoking model

Graph-theoretic tools enable a systematic investigation of the structural properties of the model. The number of directed paths which connect vertices constitutes a vital invariant for this study. The entry $A^k(i, j)$ shows the number of distinct paths which have a length of exactly $k$ that go from vertex $i$ to vertex $j$ when $A$ represents the adjacency matrix of the signal flow graph. The path counts serve as a description of the information propagation in the network, and they are utilized as a basis for various spectral measures. Furthermore, the foundational ideas can be found in [47–49]. The signal flow graph introduces new auxiliary vertices which represent lifted bilinear interaction terms that include $P_SR_S$ and $P_SV_E$ and $R_SQ_T$ to model the nonlinear transmission processes. The adjacency matrix $A(\overline{\mathscr{G}})$ of the graph formed by augmentation shows the original state variables and the lifted interaction nodes at the vertices. There is a directed edge from vertex $v_i$ to vertex $v_j$ if and only if vertex $v_i$ is a direct contributor to either the definition or the evolution of vertex $v_j$. Self-loops represent the effects of linear decay, retention, or normalization, while the auxiliary vertices reveal the nonlinear coupling pathways. The system is given access to global spectral invariants through this augmentation. The adjacency matrix for the basic augmented signal flow graph is:

$$A(\overline{\mathscr{G}}) = \begin{bmatrix} P_S & O_S & R_S & V_E & Q_T & Q_P & P_SR_S & P_SV_E & R_SQ_T \\ 1 & 0 & 0 & 0 & 0 & 0 & 1 & 1 & 0 \\ 0 & 1 & 0 & 0 & 0 & 0 & 1 & 0 & 0 \\ 0 & 1 & 1 & 1 & 0 & 0 & 0 & 0 & 1 \\ 0 & 0 & 1 & 1 & 0 & 0 & 0 & 1 & 0 \\ 0 & 0 & 1 & 1 & 1 & 0 & 0 & 0 & 1 \\ 0 & 0 & 1 & 0 & 0 & 1 & 0 & 0 & 0 \\ 1 & 1 & 0 & 0 & 0 & 0 & 0 & 0 & 0 \\ 1 & 0 & 0 & 1 & 0 & 0 & 0 & 0 & 0 \\ 0 & 0 & 1 & 0 & 1 & 0 & 0 & 0 & 0 \end{bmatrix}.$$

The self-loops that were added to the graph in order to maintain the feedback mechanisms that are already part of the equilibrium relations serve as closure for the graph. The adjacency matrix illustrates the augmented signal flow graph that has been produced as:

$$A(\mathscr{G}) = \begin{bmatrix} P_S & O_S & R_S & V_E & Q_T & Q_P & P_S R_S & P_S V_E & R_S Q_T \\ 0 & 0 & 0 & 0 & 0 & 0 & 1 & 1 & 0 \\ 0 & 0 & 0 & 0 & 0 & 0 & 1 & 0 & 0 \\ 0 & 1 & 0 & 1 & 0 & 0 & 0 & 0 & 1 \\ 0 & 0 & 1 & 0 & 0 & 0 & 0 & 1 & 0 \\ 0 & 0 & 1 & 1 & 0 & 0 & 0 & 0 & 1 \\ 0 & 0 & 1 & 0 & 0 & 0 & 0 & 0 & 0 \\ 1 & 1 & 0 & 0 & 0 & 0 & 0 & 0 & 0 \\ 1 & 0 & 0 & 1 & 0 & 0 & 0 & 0 & 0 \\ 0 & 0 & 1 & 0 & 1 & 0 & 0 & 0 & 0 \end{bmatrix}.$$

The closed signal flow graph $\mathscr{G}$ is used to investigate the spectral characteristics of the adjacency matrix $A(\mathscr{G}) \in \mathbb{R}^{9\times 9}$ in order to reveal the global connectivity and interaction structure of the system. The eigenvalues are determined by the following equation:

$$\det(\lambda I - A(\mathscr{G})) = 0,$$

yielding

$$\lambda(A(\mathscr{G})) = \left\{ \begin{array}{l} 2.05814, -1.93006, 1.55567, -1.37788, 0.895331, \\ \\ -0.713101 \pm 0.272934\,\mathrm{i}, 0.224993, 0 \end{array} \right\}.$$

The existence of a complex conjugate pair substantiates that the graph is directed and non-symmetric, thus showing irreversible information flow and cross-dimensional interaction lifting. To measure these properties, two main spectral invariants are introduced. To interpret these spectral quantities in biological terms, we consider two widely used graph invariants. The graph energy, which is defined as:

$$\mathfrak{E}(\mathscr{G}) = \sum_{i=1}^{n} |\lambda_i|,$$

The value of the computed $\mathfrak{E}(\mathscr{G})$ is found to be 9.56917, which shows that there is a very high interaction and they interact very strongly. Bio-behaviorally, a higher graph energy reflects the intensity of interactions among smoking, vaping and cessation compartments. In this context, it indicates that transitions between behavioral states (e.g., from occasional smokers to regular smokers, or from e-cigarette users to dual users) are numerous and strongly coupled, suggesting that public health interventions targeting any single compartment may trigger cascading effects across the entire population. The Estrada index is defined as:

$$\mathfrak{EE}(\mathscr{G}) = \sum_{i=1}^{n} e^{\lambda_i},$$

is evaluated as $\mathfrak{EE}(\mathscr{G}) = 18.6113$. The index measures how easily influence moves between different behavioral states throughout the entire network. The high Estrada index shows that public health organizations can effectively spread

behavioral changes which include smoking cessation and e-cigarette use through social networks and peer relationships. The research demonstrates how effective peer-led programs and social norm campaigns can be used to fight undesirable youth vaping initiation practices. The presence of complex eigenvalues leads to pure real index values because their contributions exist in conjugate pairs. The signal flow network shows extensive connectivity through its multiple feedback paths and its ability to communicate across the entire network which results in high graph energy and Estrada index values. The structural elements of this system show that its biological system maintains two separate behavioral states which operate independently from each other. The initiation of vaping increases after cigarette smoking rules change because dual use patterns affect the risk of relapse while quitting leads to changes in initiation patterns. Public health campaigns achieve better results when they tackle multiple behavioral pathways compared to staying focused on one specific behavior path. The research findings show that lifted nonlinear interaction nodes create deeper model structures which show how specific state variables dominate the system and how the system handles external disturbances.

## 7. Sensitivity analysis of $\mathscr{R}_0$'s parameters

Sensitivity analysis can be used especially when dealing with ambiguous data because it helps discover how different factors influence the stability of a model with respect to each other [50]. Moreover, it is not difficult to find out the critical process variables with this research. In search of the parameters that influence the basic reproduction number of the model positively or negatively, the paper performs a sensitivity analysis. We have the normalized forward sensitivity index (NFSI) of $\mathscr{R}_0$ is written as:

$$\Pi_p^{\mathscr{R}_0} = \frac{\partial \mathscr{R}_0}{\partial p} \times \frac{p}{\mathscr{R}_0}$$

which defines $\mathscr{R}_0$ as the basic reproduction number while $p$ includes all parameters.

$$\frac{\partial R_0}{\partial \lambda} = \frac{1}{\eta(\gamma+\varepsilon+\eta)}\left(\frac{\beta\,\alpha_1}{\alpha_1+\eta}+\frac{\beta_v\,\varepsilon}{\alpha_v+\theta+\eta}\right),$$

$$\frac{\partial R_0}{\partial \beta} = \frac{\lambda}{\eta(\gamma+\varepsilon+\eta)}\frac{\alpha_1}{\alpha_1+\eta}, \quad \frac{\partial R_0}{\partial \beta_v} = \frac{\lambda}{\eta(\gamma+\varepsilon+\eta)}\frac{\varepsilon}{\alpha_v+\theta+\eta},$$

$$\frac{\partial R_0}{\partial \alpha_1} = \frac{\lambda}{\eta(\gamma+\varepsilon+\eta)}\frac{\beta\,\eta}{(\alpha_1+\eta)^2}, \quad \frac{\partial R_0}{\partial \alpha_v} = -\frac{\lambda}{\eta(\gamma+\varepsilon+\eta)}\frac{\beta_v\,\varepsilon}{(\alpha_v+\theta+\eta)^2},$$

$$\frac{\partial R_0}{\partial \varepsilon} = \frac{\lambda}{\eta(\gamma+\varepsilon+\eta)}\frac{\beta_v(\alpha_v+\theta+\eta)-\beta_v\varepsilon}{(\alpha_v+\theta+\eta)^2} - \frac{\lambda}{\eta(\gamma+\varepsilon+\eta)^2}\left(\frac{\beta\,\alpha_1}{\alpha_1+\eta}+\frac{\beta_v\,\varepsilon}{\alpha_v+\theta+\eta}\right),$$

$$\frac{\partial R_0}{\partial \gamma} = -\frac{\lambda}{\eta(\gamma+\varepsilon+\eta)^2}\left(\frac{\beta\,\alpha_1}{\alpha_1+\eta}+\frac{\beta_v\,\varepsilon}{\alpha_v+\theta+\eta}\right),$$

$$\frac{\partial R_0}{\partial \theta} = -\frac{\lambda}{\eta(\gamma+\varepsilon+\eta)}\frac{\beta_v\,\varepsilon}{(\alpha_v+\theta+\eta)^2},$$

$$\frac{\partial R_0}{\partial \eta} = -\frac{\lambda}{\eta^2(\gamma+\varepsilon+\eta)}\left(\frac{\beta\,\alpha_1}{\alpha_1+\eta}+\frac{\beta_v\,\varepsilon}{\alpha_v+\theta+\eta}\right) - \frac{\lambda}{\eta(\gamma+\varepsilon+\eta)^2}\left(\frac{\beta\,\alpha_1}{\alpha_1+\eta}+\frac{\beta_v\,\varepsilon}{\alpha_v+\theta+\eta}\right)$$

$$-\frac{\lambda}{\eta(\gamma+\varepsilon+\eta)}\left(\frac{\beta\,\alpha_1}{(\alpha_1+\eta)^2}+\frac{\beta_v\,\varepsilon}{(\alpha_v+\theta+\eta)^2}\right).$$

Figures 3 and 4, the sensitivity indices have presented graphically. Figures 5 represents the impact of reproductive numbers is displayed. In Figures 6 and 7, we have presented impact variations of parameters on the basic reproductive number. Figures 8 and 9, 3D profiles of sensitivity indices for different values of parameters have been presented.

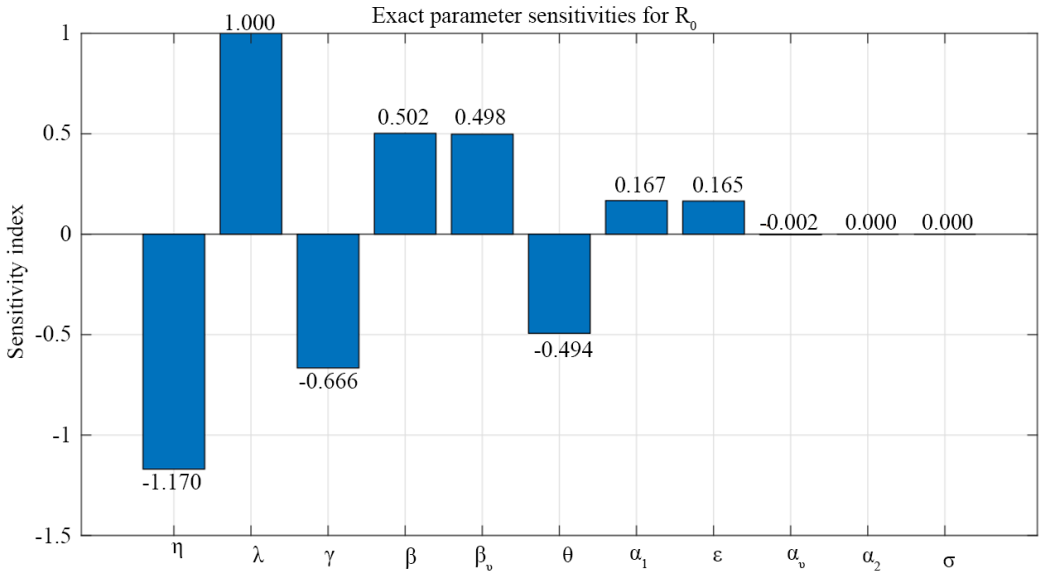


**Figure 3.** Sensitivity analysis of $\mathscr{R}_0$ for the significant parameters of model (1)

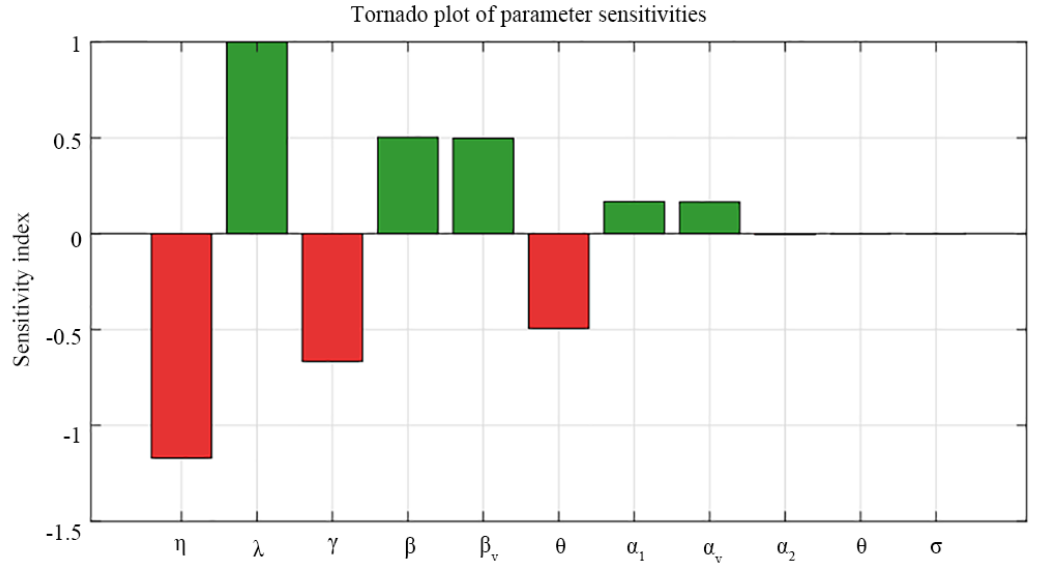


**Figure 4.** Sensitivity polarity of parameters with $\mathscr{R}_0$

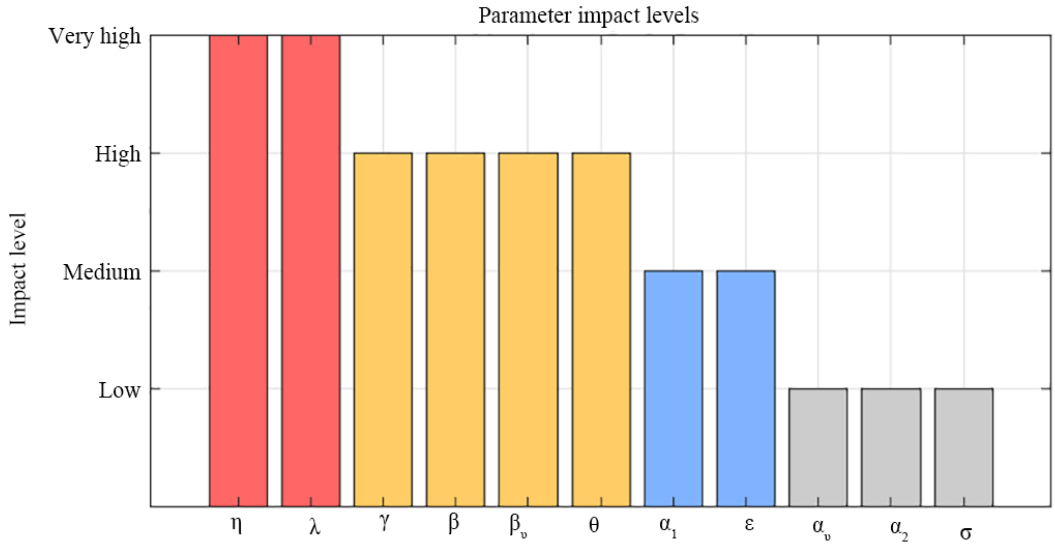


**Figure 5.** Parameters impact of $\mathscr{R}_0$

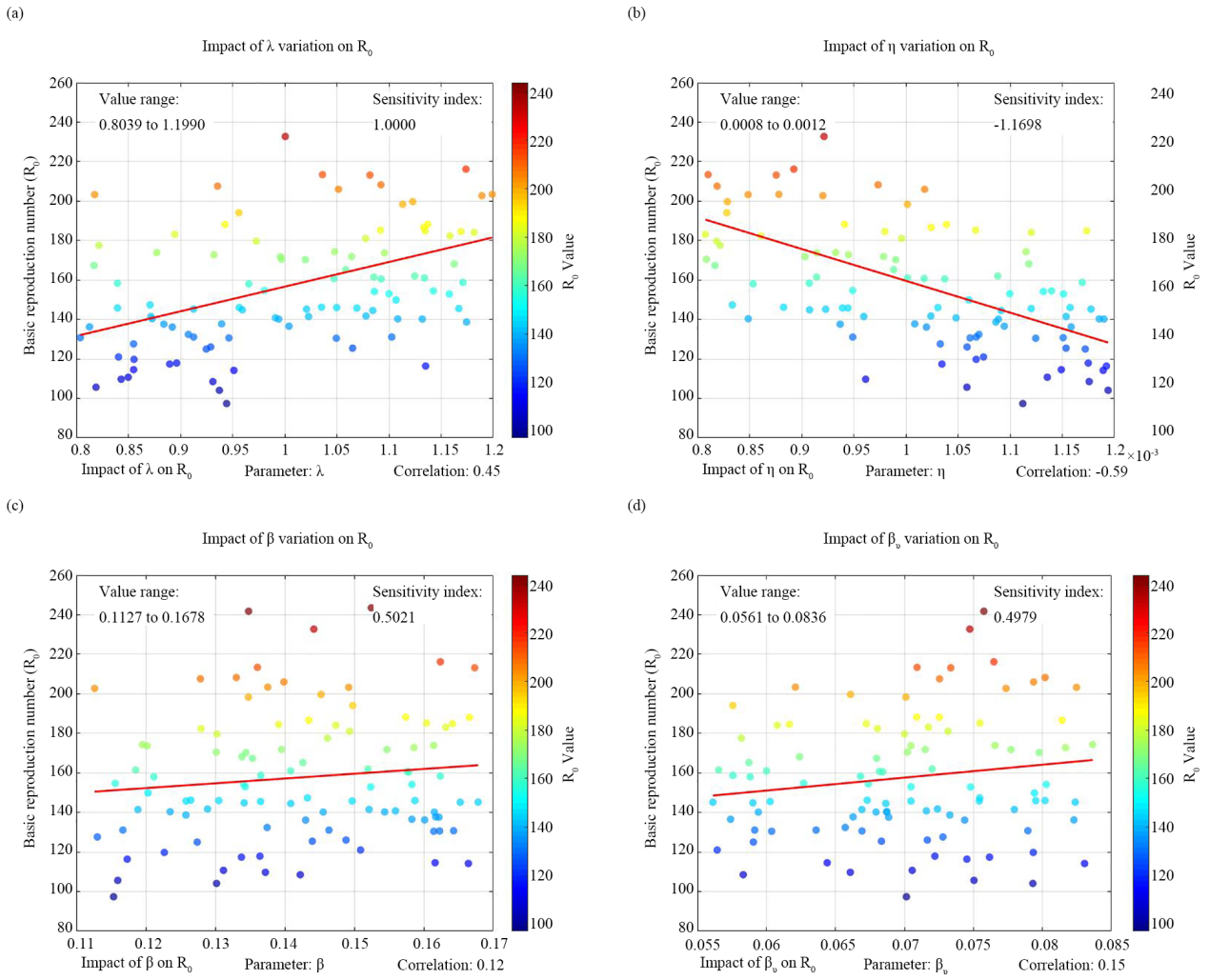

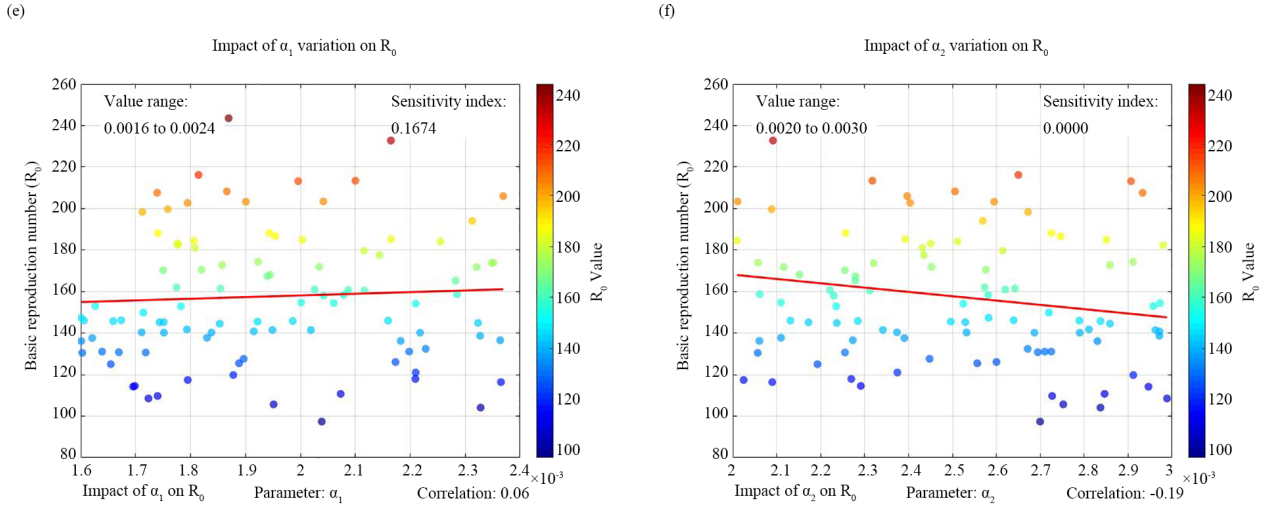


**Figure 6.** Impact variation of parameters on $\mathscr{R}_0$

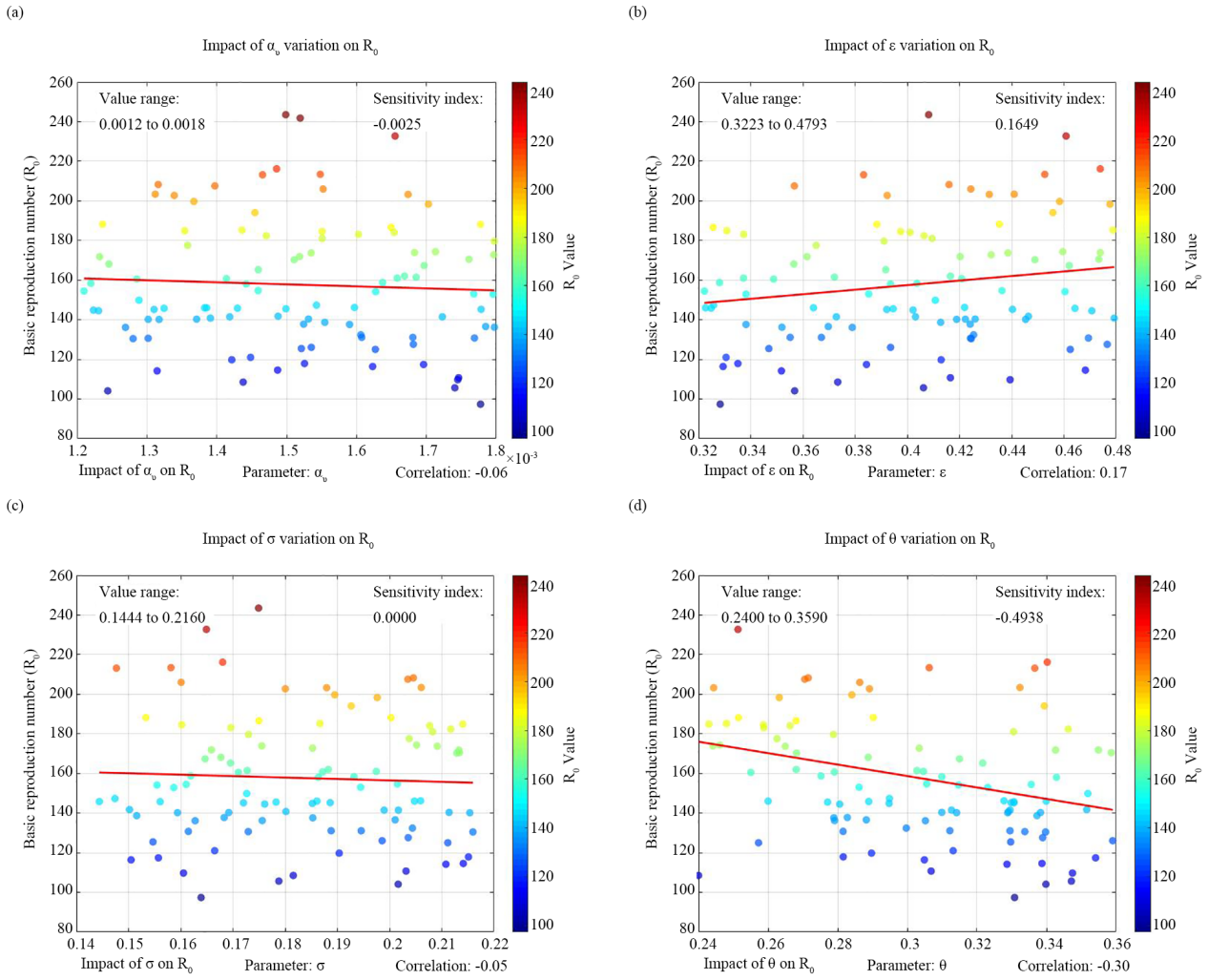


**Figure 7.** Impact variation of parameters on $\mathscr{R}_0$

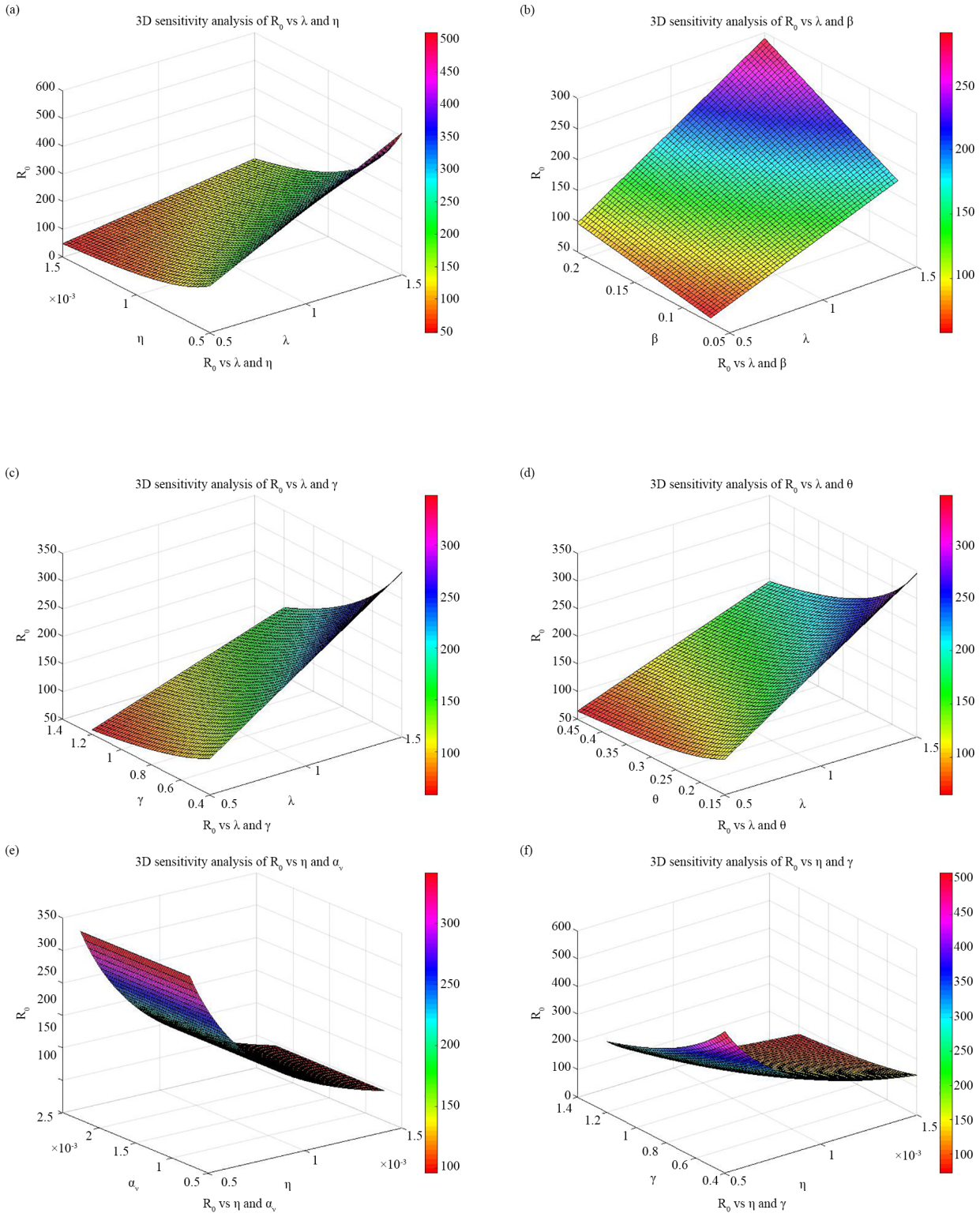


**Figure 8.** Three-dimensional sensitivity analysis of $\mathscr{R}_0$ vs different parameters

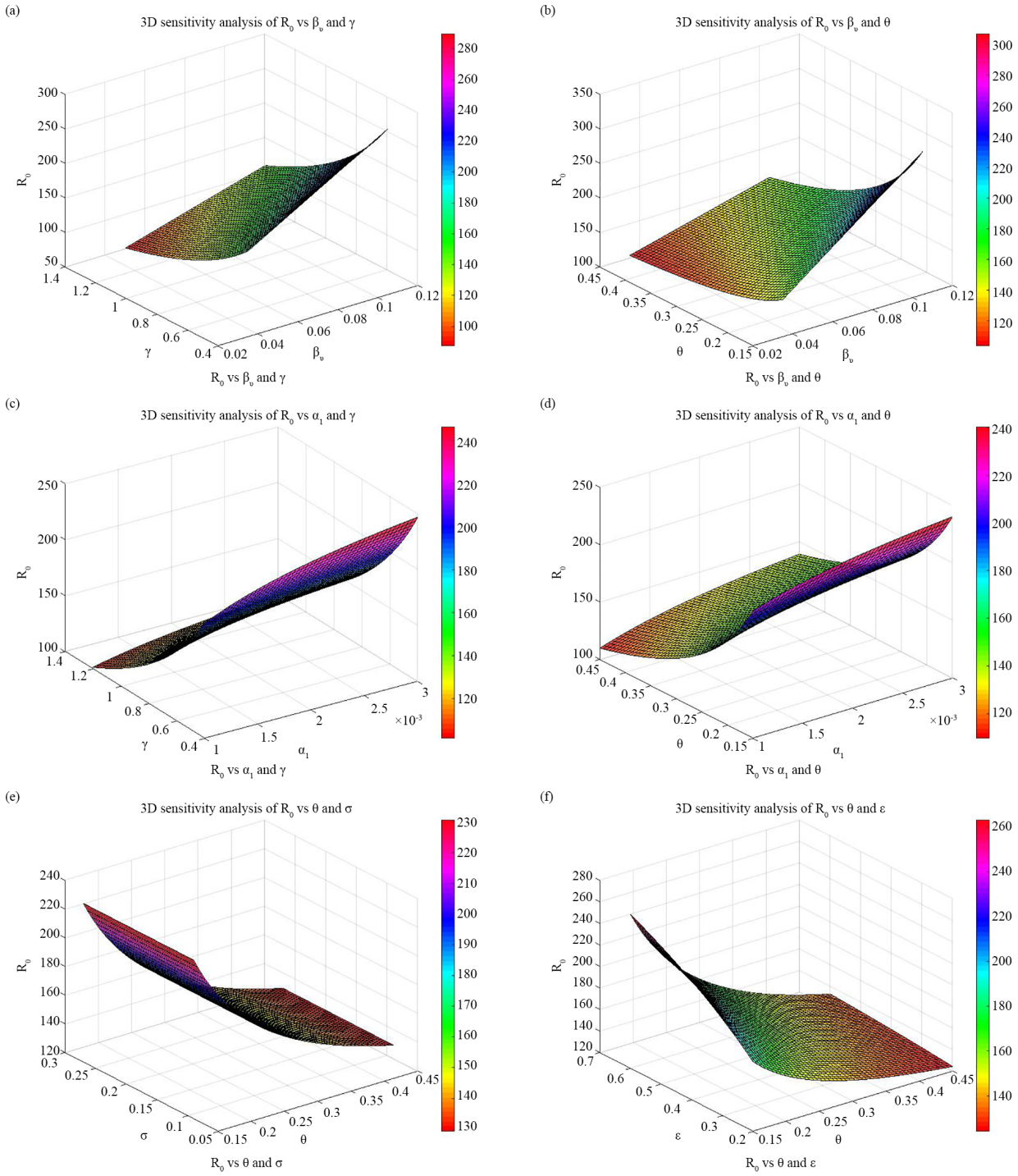


**Figure 9.** Three-dimensional sensitivity analysis of $\mathscr{R}_0$ vs different parameters

The sensitivity analysis conducted on the epidemiological model reveals important insights into the factors influencing disease transmission dynamics. The basic reproduction number $R_0 = 154.78$, indicates a highly contagious infection with significant epidemic potential. This quantity represents the average number of secondary infections generated by a single infected individual in a completely susceptible population. An $R_0$ value far exceeding unity suggests that in the absence of control measures, the disease would spread rapidly throughout the population. The study applies normalized sensitivity

analysis to reveal how changes in the parameters affect the basic reproduction number, $R_0$. The recruitment rate $\lambda$ is classified as having perfect positive sensitivity $(+1.0000)$, which means that the same percentage change in $R_0$ occurs in the same direction with every percentage change in $\lambda$. On the other hand, the natural death rate $\eta$ has the strongest negative sensitivity $(-1.1698)$ and thus, an increase in mortality would have a greater effect on the transmission potential reduction. Since both parameters have absolute sensitivity indices greater than one, they are considered to have a very high impact on disease dynamics. There are still many other parameters that have considerable influence on disease transmission, although their effect is not as much as those that were mentioned before. The recovery rate $\gamma$ has a strong negative sensitivity of $(-0.6661)$ and this implies that it is important to have effective treatment strategies in place to control the spread of the disease. The transmission coefficients $\beta$ $(+0.5021)$ and $\beta_v$ $(+0.4979)$ have similar positive sensitivities which stress the importance of reduction of contacts and mitigation of transmission. Moreover, the parameter $\theta$ that relates to increased mortality or isolation effects has also a significant negative sensitivity of $(-0.4938)$, indicating that it is an important factor in reducing $R_0$ as well. The parameters $\alpha_1$ $(+0.1674)$ and $\varepsilon$ $(+0.1649)$, both classified as having a *medium* effect, moderately influence the basic reproduction number. These parameters are associated with the stages of the disease's life cycle and hence, increase the likelihood of transmission. On the other hand, parameters like $\alpha_v$ $(-0.0025)$, $\alpha_2$ $(0.0000)$, and $\sigma$ $(0.0000)$ show almost no sensitivity, indicating that with the current parameter values, changes in these rates will have very little impact on $R_0$.

The overall sensitivity ranking acts as a major source of information for the development of efficacious intervention strategies. The factors having the highest negative sensitivities, namely $\eta$, $\gamma$ and $\theta$, are regarded as excellent possibilities for the decline in the transmittance of the disease. On the other hand, the parameters with strong positive sensitivities like $\lambda$, $\beta$ and $\beta_v$ must be controlled and supervised very carefully in order to restrict the growth of an epidemic. These results point out that the application of the most sensitive parameters for interventions is anticipated to bring about the largest mitigation of the disease spread within the limits of the proposed mathematical model.

Normalized forward sensitivity indices of the basic reproduction number have computed in Table 1 .

**Table 1.** Normalized forward sensitivity indices of the basic reproduction number $R_0$

| Parameters | Normalized sensitivity expression | Index values | Sensitivity index |
|---|---|---|---|
| $\lambda$ | $\Pi_{\lambda}^{R_0} = \frac{\partial R_0}{\partial \lambda} \cdot \frac{\lambda}{R_0}$ | +1.0000 | $+ve$ |
| $\eta$ | $\Pi_{\eta}^{R_0} = \frac{\partial R_0}{\partial \eta} \cdot \frac{\eta}{R_0}$ | −1.1698 | $-ve$ |
| $\beta$ | $\Pi_{\beta}^{R_0} = \frac{\partial R_0}{\partial \beta} \cdot \frac{\beta}{R_0}$ | +0.5021 | $+ve$ |
| $\beta_v$ | $\Pi_{\beta_v}^{R_0} = \frac{\partial R_0}{\partial \beta_v} \cdot \frac{\beta_v}{R_0}$ | +0.4979 | $+ve$ |
| $\alpha_1$ | $\Pi_{\alpha_1}^{R_0} = \frac{\partial R_0}{\partial \alpha_1} \cdot \frac{\alpha_1}{R_0}$ | +0.1674 | $+ve$ |
| $\alpha_2$ | $\Pi_{\alpha_2}^{R_0} = \frac{\partial R_0}{\partial \alpha_2} \cdot \frac{\alpha_2}{R_0}$ | 0.0000 | 0 |
| $\alpha_v$ | $\Pi_{\alpha_v}^{R_0} = \frac{\partial R_0}{\partial \alpha_v} \cdot \frac{\alpha_v}{R_0}$ | −0.0025 | $-ve$ |
| $\gamma$ | $\Pi_{\gamma}^{R_0} = \frac{\partial R_0}{\partial \gamma} \cdot \frac{\gamma}{R_0}$ | −0.6661 | $-ve$ |
| $\theta$ | $\Pi_{\theta}^{R_0} = \frac{\partial R_0}{\partial \theta} \cdot \frac{\theta}{R_0}$ | −0.4938 | $-ve$ |
| $\sigma$ | $\Pi_{\sigma}^{R_0} = \frac{\partial R_0}{\partial \sigma} \cdot \frac{\sigma}{R_0}$ | 0.0000 | 0 |
| $\varepsilon$ | $\Pi_{\varepsilon}^{R_0} = \frac{\partial R_0}{\partial \varepsilon} \cdot \frac{\varepsilon}{R_0}$ | +0.1649 | $+ve$ |

## 8. Numerical results and analysis

In this section, the numerical simulations of the smoking-vaping epidemic model executed with the fourth-order Runge-Kutta (RK4) method, are revealed. The initial conditions and biological parameters as specified in Tables 2 and 3 are used for the simulations, and the results are shown in Figures 10 and 11. The computational experiments demonstrate the time course of the complete system of six population compartments—$P_S(t)$ potential smokers, $O_S(t)$ occasional smokers, $R_S(t)$ regular smokers, $V_E(t)$ vapers, $Q_T(t)$ temporarily quit smokers and $Q_P(t)$ permanently quit smokers under two different epidemiological scenarios.

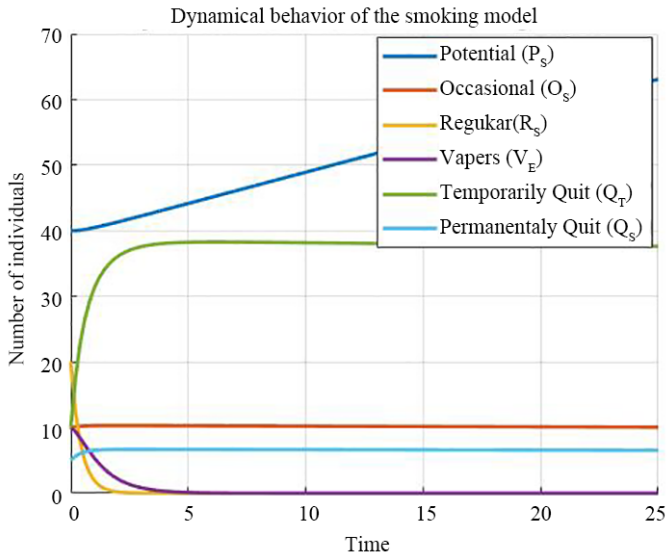


**Figure 10.** Numerical simulation of model (1) for Case 1 ($R_0 < 1$). The plot shows the dynamic behavior of all six compartments over 25 days, with the number of individuals on the vertical axis. The parameter values correspond to those listed in Table 2

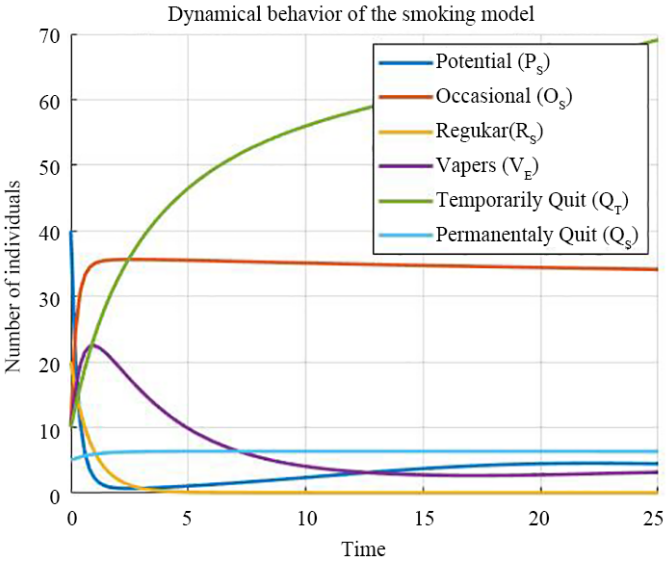


**Figure 11.** Numerical simulation of model (1) for Case 2 ($R_0 > 1$). The trajectories illustrate how higher transmission rates alter compartmental dynamics compared to Case 1. The underlying parameters are provided in Table 3

The results of the numerical simulations shown in Figures 10 and 11 reveal different epidemiological dynamics in the six-compartment smoking-vaping model for the two different sets of parameters.

In **Case 1** (Figure 10), where parameters from Table 2 result in $R_0 < 1$, the model approaches a smoking-free equilibrium. The potential smoker group $P_S(t)$ gradually increases under the constant influx of new smokers at rate $\lambda = 1$. The occasional smoker compartment $O_S(t)$ is very small due to the low smoking contact rate $\beta = 0.001$ and the slow progression rate $\alpha_1 = 0.0001$. The regular smoker compartment $R_S(t)$ declines very fast due to the high rate of smoking cessation $\gamma = 2.0$ that speeds up the process. The vapers catchment area $V_E(t)$ experiences limited expansion since it is controlled by the very low vaping contact rate $\beta_v = 0.0005$. The quitting compartments $Q_T(t)$ and $Q_P(t)$ also increase continuously. The temporarily quit population $Q_T(t)$ grows as the individuals leave smoking and vaping states, while the permanently quit group $Q_P(t)$ enlarges due to the permanent quitting fraction $\delta = 0.18$. All compartments experience a very small but consistent attrition over time due to the natural death rate $\eta = 0.001$ that is imposed.

**Table 2.** Parameter values for Case 1: $R_0 < 1$ (smoking-free equilibrium stable)

| Symbol | Description | Value (1/day) | Source |
|---|---|---|---|
| $\lambda$ | Recruitment rate into potential smoking | 1 | Estimated |
| $\eta$ | Natural death rate | 0.001 | Estimated |
| $\beta$ | Smoking contact rate | 0.001 | [34] |
| $\beta_v$ | Vaping contact rate | 0.0005 | Estimated |
| $\alpha_1$ | Smoking progression rate | 0.0001 | Estimated |
| $\alpha_2$ | Relapse rate | 0.0025 | [35] |
| $\alpha_v$ | Gateway rate (vaping to smoking) | 0.0015 | Estimated |
| $\gamma$ | Smoking quitting rate | 2.0 | [34] |
| $\theta$ | Vaping quitting rate | 1.0 | [51] |
| $\delta$ | Permanent quitting fraction | 0.18 | [34] |
| $\varepsilon$ | Switching rate (smoking to vaping) | 0.4 | Estimated |

In **Case 2** (Figure 11), with parameters from Table 3 producing $R_0 > 1$, the dynamics shift dramatically toward an endemic smoking equilibrium. The combination of elevated smoking contact rate $\beta = 0.14$ together with the progression rate $\alpha_1 = 0.002$ results in substantial growth through the regular smoker compartment $R_S(t)$. The occasional smoker group $O_S(t)$ acts as an intermediate reservoir, feeding into regular smoking. The vaper population $V_E(t)$ also expands significantly because of the higher vaping contact rate $\beta_v = 0.07$ and the switching rate $\varepsilon = 0.4$ from smoking to vaping. The potential smoker pool $P_S(t$ experiences accelerated depletion because individuals progress into both smoking and vaping behaviors. The quitting compartments $Q_T(t)$ exhibit slower growth compared to Case 1 because the quitting rates have decreased to $\gamma = 0.8$ for smoking and $\theta = 0.3$ for vaping. The permanently quit population $Q_P(t)$ maintains a gradual growth pattern that shows how difficult it is to stay off drugs in an area with high transmission rates. The natural mortality rate $\eta = 0.001$ operates as a constant exit mechanism which leads to gradual compartment size reduction throughout both scenarios. The model uses the relapse rate $\alpha_2 = 0.0025$ together with the gateway rate $\alpha_v = 0.0015$ to show how smoking and vaping interact. The model demonstrates its ability to depict real-world complexities through its representation of gateway and dual-use behaviors while demographic shifts in the population continue with $\eta$. The researchers established parameter values from established mathematical models of smoking and vaping which appear in Tables 2 and 3. Two sets of parameters were applied to investigate the model's behavior under different epidemiological conditions. The model was tested under two different epidemiological regimes, which were labelled as Case 1 and Case 2. The initial conditions were the same in both cases and were set as follows:

$$(P_S(0), O_S(0), V_E(0), R_S(0), Q_T(0), Q_P(0)) = (40, 10, 20, 10, 10, 5),$$

keeping the overall population steady. The integration of numbers was done with a fractional differential equation solver in MATLAB. In the first case, with the parameters from table 2, the basic reproduction number $R_0^{(1)} \approx 0.121$ is calculated as:

$$R_0 = \frac{\lambda}{\eta(\gamma+\varepsilon+\eta)}\left(\frac{\beta\,\alpha_1}{\alpha_1+\eta} + \frac{\beta_v\,\varepsilon}{\alpha_v+\theta+\eta}\right)$$

Since $R_0 < 1$, the smoking-free equilibrium is stable which means that smoking would eventually get extinct in the population with the specified parameters. On the other hand, in Case 2, the scenario with higher transmission rates as shown in Table 3 results in $R_0^{(2)} \approx 154.78 > 1$, and therefore, an endemic state of smoking. The graphical representations in Figures 10 and 11 provide a clear distinction between these two scenarios and, thus, bring forth visual proof of the threshold behavior ruled by $R_0$ and give useful public health intervention planning insights.

**Table 3.** Parameter values for Case 2: $R_0 > 1$ (endemic smoking equilibrium)

| Symbol | Description | Value (1/day) | Source |
|---|---|---|---|
| $\lambda$ | Recruitment rate into potential smoking | 1 | Estimated |
| $\eta$ | Natural death rate | 0.001 | Estimated |
| $\beta$ | Smoking contact rate | 0.14 | [34] |
| $\beta_v$ | Vaping contact rate | 0.07 | Estimated |
| $\alpha_1$ | Smoking progression rate | 0.002 | [33] |
| $\alpha_2$ | Relapse rate | 0.0025 | [35] |
| $\alpha_v$ | Gateway rate (vaping to smoking) | 0.0015 | Estimated |
| $\gamma$ | Smoking quitting rate | 0.8 | [34] |
| $\theta$ | Vaping quitting rate | 0.3 | [51] |
| $\delta$ | Permanent quitting fraction | 0.18 | [34] |
| $\varepsilon$ | Switching rate (smoking to vaping) | 0.4 | Estimated |

## 9. Simulation framework using simulink

The study of the dynamic behavior of the fractional-order smoking model (1) was carried out using a MATLAB Simulink-based comprehensive simulation environment. The system of differential equations can be simulated and analyzed through this modeling method which uses block diagrams as its visual modeling tool. The simulink model illustrated in Figure 12 is the computational engine for simulating the dynamics of the epidemic. The system enables numerical integration of mathematical model elements which include complex social interactions and fractional-order derivative functions over a defined time period. The block diagram shows each smoking population compartment as a separate subsystem which uses continuous feedback loops to model the group's transition rates and nonlinear connections between different populations.

After the system-level simulation process, the temporal evolution of each single population compartment was obtained and displayed. The time-series data resulting from all six state variables is shown in Figure 13, which gives a comprehensive

view of the smoking epidemic model's progression. The analysis of the compartmental trajectories provide the system with valuable insights. The graph showing the potential smokers, (Figure 13a), indicates the transition of individuals from this state to others which is the reason why the curve gets downwards. The occasional smokers, (Figure 13b), on the other hand, might get to maximums before the final fall, that meaning shorttime smoking involvement. The regular smokers group (Figure 13c), seems to be growing and leveling off, the main reasons being baptism and quitting.

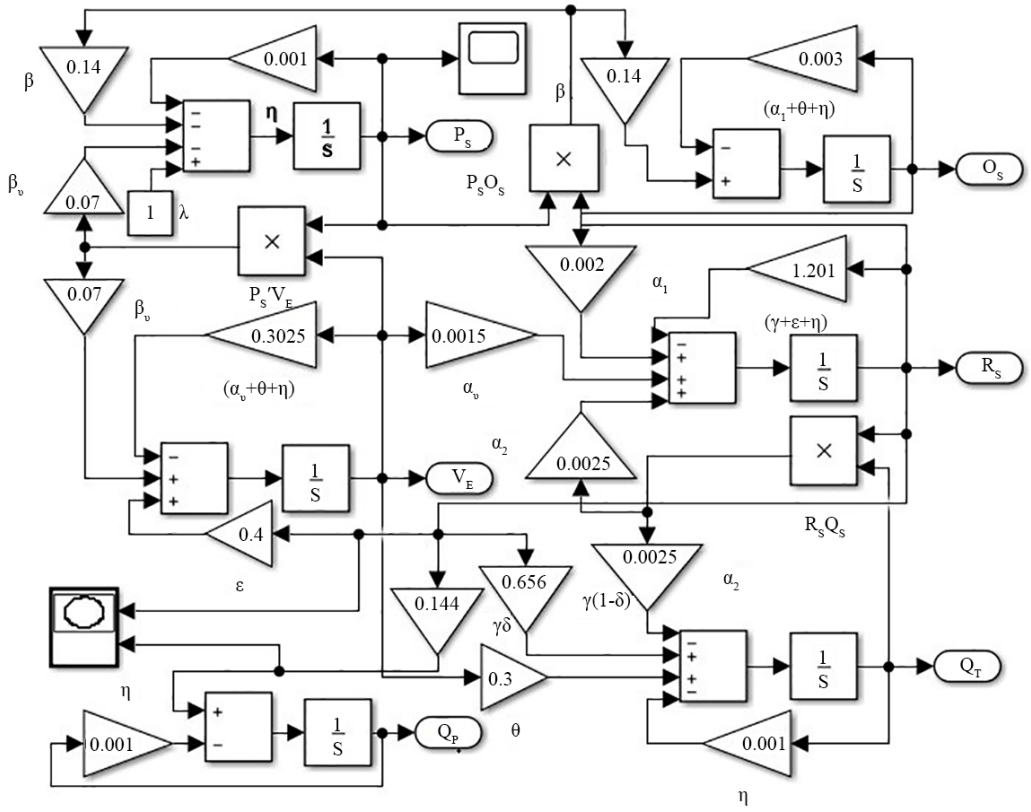


**Figure 12.** Simulink block diagram of model (1)

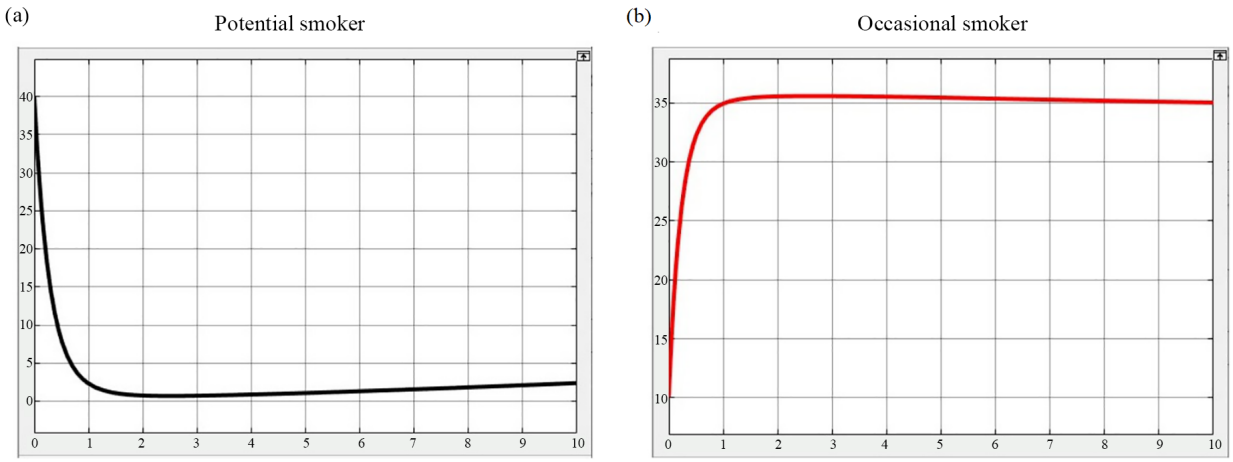

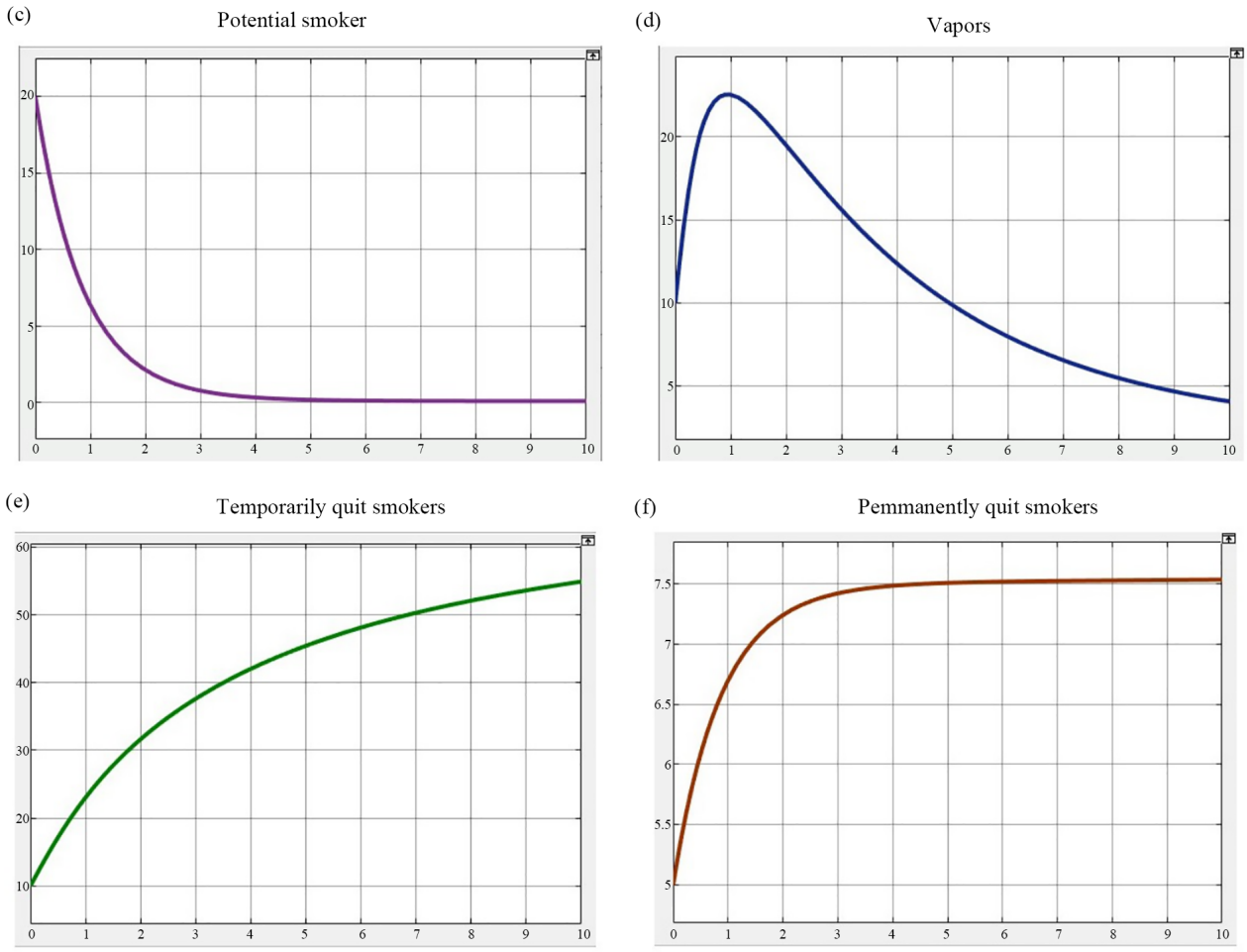


**Figure 13.** Simulink graphs of compartments

The vapers, (Figure 13d), undergo transformations based on the current ways of nicotine consumption, while the temporarily quitters, (Figure 13e), and the permanently quitters, (Figure 13f) populations present the healing routes within the model. All these graphs together not only prove the correctness of the developed model but also provide a basis for determining intervention and parameter sensitivity strategies in the simulated smoking epidemic.

## 10. Conclusion

This paper has introduced a new mathematical model that is vast and comprehensive for defining the smoking and vaping dynamics that are interlinked together and happening in a single population at the same time. Unlike the traditional methods that consider these behavior separately, the new model is able to depict their co-development as well as their complex interactions. Initially, the analysis was performed in the usual integer-order framework, where the main qualitative characteristics of the system, such as positivity, boundedness, and the presence and uniqueness of solutions were established rigorously. The non-infected and infected equilibrium points were obtained, and the basic reproduction number was derived using the next-generation matrix method. Both local and global stability characteristics were studied, resulting in straightforward threshold criteria that define the long-term behavior of the system. In addition, a sensitivity analysis of the reproduction number was performed to reveal the most significant parameters, thus providing useful guidance for the development of efficient prevention and control measures. The researchers used a signal flow graph together with spectral

analysis to explain the model's structural connectivity. The researchers used graph energy and Estrada index calculations to measure interaction strength and global network communicability throughout the behavioral network. The biological interpretation of spectral measures showed that higher graph energy measured the strong connection between smoking and vaping and cessation pathways while the Estrada index showed the social networks efficiency in spreading behavioral influence which demonstrated the effectiveness of peer-led programs. The numerical simulations performed in MATLAB demonstrated actual results which matched the theoretical outcomes while displaying multiple nonlinear dynamic behaviors across various parameter settings. The model incorporates demographic variability through the recruitment term $\lambda$ and the natural death rate $\eta$ applied uniformly across all compartments, which results in total population growth according to the equation $\frac{dN}{dt} = \lambda - \eta N$ and the population reaching its demographic equilibrium. The mathematical structure of the system uses mass-action-like terms that resemble chemical kinetics yet the system directly represents peer pressure and social norms and personal choice as drivers of behavioral changes which the model uses to study behavioral epidemiology and social contagion theory. The research results show different directions which researchers can pursue for future research work. The study needs to be expanded through age-structured and gender-structured population research which will establish more realistic demographic patterns of smoking and vaping. The study needs to incorporate spatial diffusion and network-based interaction methods which will enable research on how geographical and social factors affect these behaviors. The model requires the introduction of Atangana-Baleanu and Caputo-Fabrizio and variable-order derivatives as fractional operators which will enhance its memory capabilities and enable it to model complex persistence behavior. The study needs to include optimal control strategies as a beneficial addition which will enable researchers to create and assess cost-efficient intervention strategies that include public awareness campaigns and taxation systems and rehabilitation programs. The proposed modeling and prediction framework will assist public health authorities because they can use it to assess how regulatory policies and prevention measures and treatment strategies impact public health. The same approach may also be applied to other complex behavioral or epidemiological systems, e.g. alcohol addiction, drug abuse, or multi-behavior epidemic models, where memory effects, nonlinear interactions, and data-driven prediction are essential.

## Acknowledgement

Authors are thankful to Prince Sultan University for APC and support through TAS research lab.

## Confilict of interest

The authors declare no competing financial interest.

## References

[1] Li Y, Hecht SS. Carcinogenic components of tobacco and tobacco smoke: a 2022 update. *Food and Chemical Toxicology*. 2022; 165: 113179. Available from: https://doi.org/10.1016/j.fct.2022.113179.

[2] Van den Driessche P, Watmough J. Reproduction numbers and sub-threshold endemic equilibria for compartmental models of disease transmission. *Mathematical Biosciences*. 2002; 180(1–2): 29–48. Available from: https://doi.org/10.1016/S0025-5564(02)00108-6.

[3] Jha P. Smoking cessation and e-cigarettes in China and India. *BMJ*. 2019; 367. Available from: https://doi.org/10.1136/bmj.l6013.

[4] Boutayeb A, Boutayeb S. The burden of non communicable diseases in developing countries. *International Journal for Equity in Health*. 2005; 4: 1–8. Available from: https://doi.org/10.1186/1475-9276-4-2.

[5] Anand K, Shah B, Yadav K, Singh R, Mathur P, Paul E, Kapoor SK. Are the urban poor vulnerable to non-communicable diseases? A survey of risk factors for non-communicable diseases in urban slums of Faridabad. *National Medical Journal of India*. 2007; 20(3): 115.

[6] Khyar O, Danane J, Allali K. Mathematical analysis and optimal control of giving up the smoking model. *International Journal of Differential Equations*. 2021; 2021(1): 8673020. Available from: https://doi.org/10.1155/2021/8673020.

[7] Zeb A, Zaman G, Momani S. Square-root dynamics of a giving up smoking model. *Applied Mathematical Modelling*. 2013; 37(7): 5326–5334. Available from: https://doi.org/10.1016/j.apm.2012.10.005.

[8] Franck C, Budlovsky T, Windle SB, Filion KB, Eisenberg MJ. Electronic cigarettes in North America: history, use, and implications for smoking cessation. *Circulation*. 2014; 129(19): 1945–1952. Available from: https://doi.org/10.1161/CIRCULATIONAHA.113.006416.

[9] Krishnasamy VP, Hallowell BD, Ko JY, Board A, Hartnett KP, Salvatore PP, et al. Update: characteristics of a nationwide outbreak of e-cigarette, or vaping, product use-associated lung injury—United States, August 2019–January 2020. *MMWR Morbidity and Mortality Weekly Report*. 2020; 69(3): 90. Available from: https://doi.org/10.15585/mmwr.mm6903e2.

[10] Miyashita L, Foley G. E-cigarettes and respiratory health: the latest evidence. *Journal of Physiology*. 2020; 598(22): 5027–5038. Available from: https://doi.org/10.1113/JP279526.

[11] Eaton DL, Kwan LY, Stratton K. *Public Health Consequences of E-Cigarettes*. Washington, DC: National Academies Press; 2018. Available from: https://doi.org/10.17226/24952.

[12] Owusu D, Huang J, Weaver SR, Pechacek TF, Ashley DL, Nayak P, et al. Patterns and trends of dual use of e-cigarettes and cigarettes among U.S. adults, 2015-2018. *Preventive Medicine Reports*. 2019; 16: 101009. Available from: https://doi.org/10.1016/j.pmedr.2019.101009.

[13] Osei AD, Mirbolouk M, Orimoloye OA, Bhatnagar A, Nasir K, Blaha MJ, et al. Association between e-cigarette use and cardiovascular disease among never and current combustible-cigarette smokers. *The American Journal of Medicine*. 2019; 132(8): 949–954.e2. Available from: https://doi.org/10.1016/j.amjmed.2019.02.016.

[14] Parekh T, Pemmasani S, Desai R. Risk of stroke with e-cigarette and combustible cigarette use in young adults. *American Journal of Preventive Medicine*. 2020; 58(3): 446–452. Available from: https://doi.org/10.1016/j.amepre.2019.10.008.

[15] Wang JB, Olgin JE, Nah G, Vittinghoff E, Cataldo JK, Pletcher MJ, et al. Cigarette and e-cigarette dual use and risk of cardiopulmonary symptoms in the Health eHeart Study. *PLoS ONE*. 2018; 13(7): e0198681. Available from: https://doi.org/10.1371/journal.pone.0198681.

[16] Abafalvi L, Pénzes M, Urbán R, Foley KL, Kaán R, Kispélyi B, et al. Perceived health effects of vaping among Hungarian adult e-cigarette-only and dual users: a cross-sectional internet survey. *BMC Public Health*. 2019; 19(1): 302. Available from: https://doi.org/10.1186/s12889-019-6629-0.

[17] Cobb CO, Foulds J, Yen MS, Veldheer S, Lopez AA, Yingst JM, et al. Effect of an electronic nicotine delivery system with 0, 8, or 36 mg/mL liquid nicotine versus a cigarette substitute on tobacco-related toxicant exposure: a four-arm, parallel-group, randomised, controlled trial. *The Lancet Respiratory Medicine*. 2021; 9(8): 840–850. Available from: https://doi.org/10.1016/S2213-2600(21)00022-9.

[18] Straughan B. E-cigarette smoking with peer pressure. *Mathematical Methods in the Applied Sciences*. 2019; 42(6): 2098–2108. Available from: https://doi.org/10.1002/mma.5503.

[19] Uçar E, Uçar S, Evirgen F, Özdemir N. Investigation of e-cigarette smoking model with Mittag-Leffler kernel. *Mathematical Methods in the Applied Sciences*. 2021; 46(1): 98–109. Available from: https://doi.org/10.2478/fcds-2021-0007.

[20] Funk S, Salathé M, Jansen VA. Modelling the influence of human behaviour on the spread of infectious diseases: a review. *Journal of the Royal Society Interface*. 2010; 7(50): 1247–1256. Available from: https://doi.org/10.1098/rsif.2010.0142.

[21] Alesina A, Giavazzi F, Favero C. *Austerity: When It Works and When It Doesn't*. Princeton University Press; 2019.

[22] Gerace F, Krzakala F, Loureiro B, Stephan L, Zdeborová L. Gaussian universality of perceptrons with random labels. *Physical Review E*. 2024; 109(3): 034305. Available from: https://doi.org/10.1103/PhysRevE.109.034305.

[23] Chu YM, Zafar ZUA, Inc M, Javeed S, Ali AS. Numerical modeling of a novel stochastic coronavirus. *Fractals*. 2022; 30(08): 2240211. Available from: https://doi.org/10.1142/S0218348X22402113.

[24] Ali AS, Javeed S, Faiz Z, Baleanu D. Mathematical modelling, analysis and numerical simulation of social media addiction and depression. *PLOS ONE*. 2024; 19(3): e0293807. Available from: https://doi.org/10.1371/journal.pone.0293807.

[25] Faiz Z, Javeed S, Ahmed I, Baleanu D, Riaz MB, Sabir Z. Numerical solutions of the Wolbachia invasive model using Levenberg-Marquardt backpropagation neural network technique. *Results in Physics*. 2023; 50: 106602. Available from: https://doi.org/10.1016/j.rinp.2023.106602.
[26] Murray JD. *Mathematical Biology: I. An Introduction*. New York: Springer; 2002. Volume 17. Available from: https://doi.org/10.1007/b98868.
[27] Sahu GP, Dhar J. Analysis of an SVEIS epidemic model with partial temporary immunity and saturation incidence rate. *Applied Mathematical Modelling*. 2012; 36(3): 908–923. Available from: https://doi.org/10.1016/j.apm.2011.07.037.
[28] Hethcote HW, van den Driessche P. Some epidemiological models with nonlinear incidence. *Journal of Mathematical Biology*. 1991; 29(3): 271–287. Available from: https://doi.org/10.1007/BF00160539.
[29] Parsamanesh M, Erfanian M. Global dynamics of a mathematical model for propagation of infection diseases with saturated incidence rate. *Journal of Advanced Mathematical Modelling*. 2021; 11(1): 69–81. Available from: https://doi.org/10.22055/jamm.2020.33801.1822.
[30] Khan H, Alzabut J, Shah A, Etemad S, Rezapour S, Park C. A study on the fractal-fractional tobacco smoking model. *AIMS Mathematics*. 2022; 7(8): 13887–13909. Available from: https://doi.org/10.3934/math.2022767.
[31] Shah A, Khan H, De la Sen M, Alzabut J, Etemad S, Deressa CT, Rezapour S. On non-symmetric fractal-fractional modeling for ice smoking: mathematical analysis of solutions. *Symmetry*. 2022; 15(1): 87. Available from: https://doi.org/10.3390/sym15010087.
[32] Khan H, Alzabut J, Gómez-Aguilar JF, Alkhazan A. Essential criteria for existence of solution of a modified-ABC fractional order smoking model. *Ain Shams Engineering Journal*. 2024; 15(5): 102646. Available from: https://doi.org/10.1016/j.asej.2024.102646.
[33] Neale M, Harvey E, Maes H, Sullivan PF, Kendler KS. Extensions to the modeling of initiation and progression: applications to substance use and abuse. *Behavior Genetics*. 2006; 36(4): 507–524. Available from: https://doi.org/10.1007/s10519-006-9063-x.
[34] Sharomi O, Gumel AB. Curtailing smoking dynamics: a mathematical modeling approach. *Applied Mathematics and Computation*. 2008; 195(2): 475–499. Available from: https://doi.org/10.1016/j.amc.2007.05.012.
[35] Alkhudhari Z, Al-Sheikh S, Al-Tuwairqi S. Global dynamics of a mathematical model on smoking. *International Scholarly Research Notices*. 2014; 2014(1): 847075. Available from: https://doi.org/10.1155/2014/847075.
[36] Sofia IR, Bandekar SR, Ghosh M. A mathematical model on smoking dynamics in society with relapse. *Quality & Quantity*. 2026; 60: 2999–3023. Available from: https://doi.org/10.1007/s11135-025-02385-3.
[37] Numpanviwat N, Pholuang J. Mathematical analysis of a smoking model with anti-smoking campaign rate in Thailand. *Journal of Applied Research on Science and Technology (JARST)*. 2026; 25(1): 261964. Available from: https://doi.org/10.60101/jarst.2026.261964.
[38] Zhao J, Ma L. Threshold dynamics and optimal control of an epidemiological smoking model. *Nonlinear Engineering*. 2025; 14(1): 20250153. Available from: https://doi.org/10.1515/nleng-2025-0153.
[39] Noersena A, Fatmawati F, Alfiniyah C, Abidemi A. Mathematical modelling of smoking behavior: treatment and prevention optimal control. *Barekeng*. 2025; 19(3): 2003–2016. Available from: https://doi.org/10.30598/barekengvol19iss3pp2003-2016.
[40] Bushnaq S, Bano S, Zeb A. Analysis of a smoking dynamics model with age-dependent incidence function. *European Journal of Pure and Applied Mathematics*. 2025; 18(3): 6447–6447. Available from: https://doi.org/10.29020/nybg.ejpam.v18i3.6447.
[41] Ansori MF. A discrete-time mathematical model of smoking dynamics with two sub-populations of smokers. *Journal of Mathematical Epidemiology*. 2025; 1(1): 11–25. Available from: https://doi.org/10.64891/jome.3.
[42] Perko L. *Differential Equations and Dynamical Systems*. New York: Springer; 2001. Available from: https://doi.org/10.1007/978-1-4613-0003-8.
[43] Van den Driessche P, Watmough J. Reproduction numbers and sub-threshold endemic equilibria for compartmental models of disease transmission. *Mathematical Biosciences*. 2002; 180(1–2): 29–48. Available from: https://doi.org/10.1016/S0025-5564(02)00108-6.
[44] Korobeinikov A, Wake GC. Lyapunov functions and global stability for SIR, SIRS, and SIS epidemiological models. *Applied Mathematics Letters*. 2002; 15(8): 955–960. Available from: https://doi.org/10.1016/S0893-9659(02)00069-1.
[45] Brouwer AE, Haemers WH. *Spectra of Graphs*. New York: Springer; 2012. Available from: https://doi.org/10.1007/978-1-4614-1939-6.

[46] Schmid H, Huber A. Analysis of switched-capacitor circuits using driving-point signal-flow graphs. *Analog Integrated Circuits and Signal Processing*. 2018; 96(3): 495–507. Available from: https://doi.org/10.1007/s10470-018-1131-7.

[47] Mahdy AMS, Sweilam NH, Higazy M. Approximate solution for solving nonlinear fractional-order smoking model. *Alexandria Engineering Journal*. 2020; 59(2): 739–752. Available from: https://doi.org/10.1016/j.aej.2020.01.049.

[48] Mahdy AMS, Higazy M, Gepreel KA, El-Dahdouh AAA. Optimal control and bifurcation diagram for a nonlinear fractional SIRC model. *Alexandria Engineering Journal*. 2020; 59(5): 3481–3501. Available from: https://doi.org/10.1016/j.aej.2020.05.028.

[49] De La Peña JA, Gutman I, Rada J. Estimating the Estrada index. *Linear Algebra and Its Applications*. 2007; 427(1): 70–76. Available from: https://doi.org/10.1016/j.laa.2007.06.020.

[50] Goswami NK, Olaniyi S, Abimbade SF, Chuma FM. A mathematical model for investigating the effect of media awareness programs on the spread of COVID-19 with optimal control. *Health Analytics*. 2024; 5: 100300. Available from: https://doi.org/10.1016/j.health.2024.100300.

[51] Machado-Marques SI, Moyles IR. Adolescent vaping behaviours: exploring the dynamics of a social contagion model. *Mathematical Biosciences*. 2024; 377: 109303. Available from: https://doi.org/10.1016/j.mbs.2024.109303.